Master Thesis, Department of Geosciences

Geology, geochemistry and geochronology of Neoproterozoic rocks in western Shire, Northern Ethiopia

Gebreyohannes, Gebrehiwet Welay

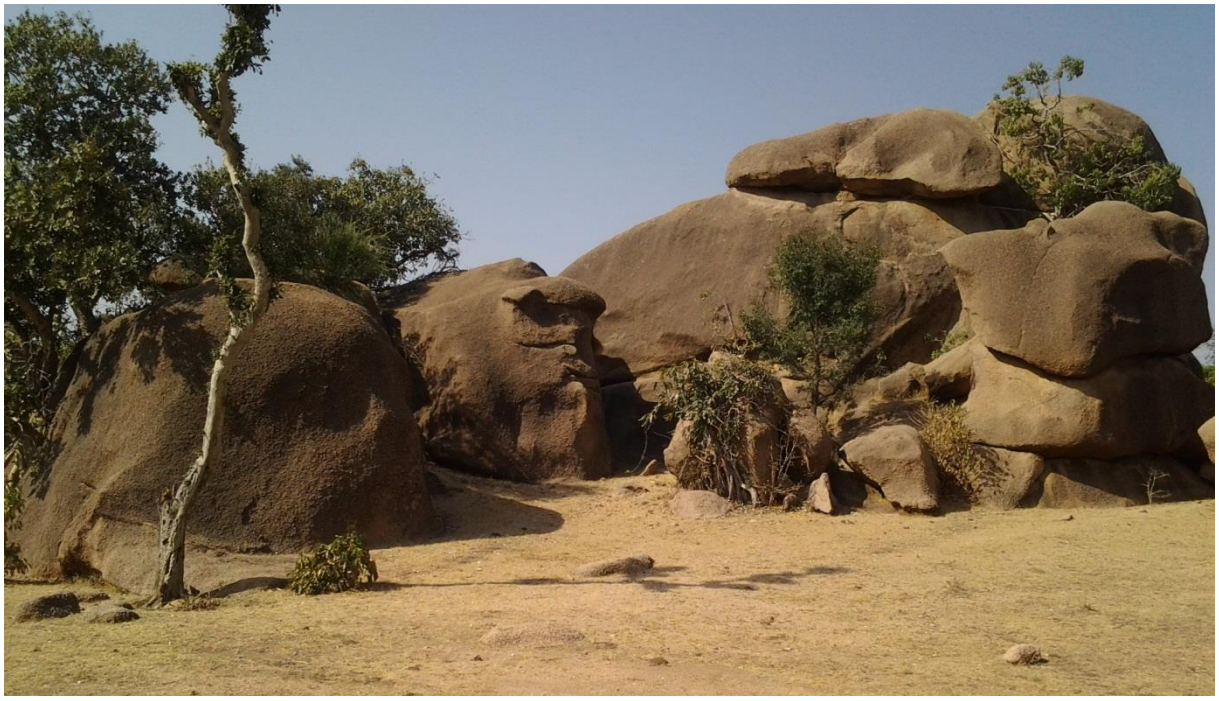

UNIVERSITY OF OSLO

FACULTY OF MATHEMATICS AND NATURAL SCIENCES

Geology, geochemistry and geochronology of Neoproterozoic rocks in western Shire, Northern Ethiopia

Gebreyohannes, Gebrehiwet Welay

Master Thesis in Geosciences

Discipline: Geology of mineral resources

Department of Geosciences

Faculty of Mathematics and Natural Sciences

University of Oslo

September, 2014

Supervisor: **Professor Fernando Corfu**

This work is published digitally through DUO – Digitale Utgivelser ved UiO
http://www.duo.uio.no
It is also catalogued in BIBSYS (http://www.bibsys.no/english)

ABSTRACT

The study area is situated within the northern Ethiopian Precambrian shield terrain largely of sutured low-grade assemblages of Neo-Proterozoic volcanic, volcano-sedimentary which belongs to the Tsaliet and Tambien Groups in the southern most Arabian Nubian Shield (ANS). This thesis represents the findings concerning 8 rock samples from western Shire in Tigray region. The samples represent three specific locations such as Hitsas, Gurungur and Kisad Gaba. The objectives of this study were to carry out geological, geochronological (zircon and titanite U-Pb) and geochemical studies to determine the geological and tectonic settings, geochemistry and emplacement time of the granites. The samples were studied using Isotope Dilution-Thermal Ionization Mass Spectroscopy (ID-TIMS), Fusion- Inductively Coupled Plasma (FUS-ICP) and Fusion- Mass Spectrometry (FUS-MS). The studied area is dominated by metavolcanics, sericite quartz-feldspar schist, phyllitic and graphitic schist, mafic -ultramafic rocks, sedimentary rocks, and granitic intrusives traversed by pegmatites and quartz veins, and mafic-felsic dykes. Zircon and titanite U-Pb age dates indicate that the Hitsas pluton is emplaced at about 627.5 ± 1.1 Ma, that of the Gurungur granite is at about 624.24±0.60Ma, and that of the Kisad Gaba granite is at about 606.1 ± 2.6 Ma and 610.7 ± 1.1Ma coeval with the juvenile Neoproterozoic rocks in the ANS, identified until present. Geochemically, the studied granites and metavolcanic rocks are similar to medium to high-K calc-alkaline rocks characterized by high SiO_2, high total alkali concentrations (8.22-8.97 wt. %) and displaying the predominance of K_2O over Na_2O. The negative correlation SiO_2 with Al_2O_3, Fe_2O_3, CaO, TiO_2, and P_2O_5 and positive correlation with K_2O and Na_2O indicate fractionation nature of these granitic and metavolcanic rocks during magmatic differentiation. The enrichment of large ion lithophile elements, depletion of high field strength elements indicates a partial melting and crustal contamination of magma above subduction zones or volcanic arc and syn to post-collisional granitoids. They are I-type, strongly peraluminous with S-type features, enriched in light rare earth elements relative to heavy rare earth elements and have fractionated rare earth element patterns ((La/Yb)N= 10.24-40.24)). Thus we conclude that studied granites and metavolcanic rocks are I-type generated from mantle –crust source. The negative anomalies of Nb, Ti and P might indicate a subduction related origin. I-type granites are enriched in Ba, K, Th and depleted in Nb and Zr suggesting the interaction with the crustal materials. I-type granitoids may also resulted from a contamination of mantle-derived magmas by a partial melting of crustal materials in subduction zones.

ACKNOWLEDGEMENTS

I would like to thank the Norwegian Quota Scheme scholarship program for giving me the opportunity to study and do this Master thesis at the University Of Oslo.

I would like to thank my supervisor Professor Fernando Corfu for his continuous and extraordinary help, follow up, and guidance that he dedicated to me from the beginning to the end of my studies. This work could not have been complete without his significant efforts, constructive criticisms, during the field works and discussions.

I would also like to acknowledge the technical staff at the department of Geosciences providing the entire necessary laboratory to conduct my research. Appreciation is extends to my all friends whom they advise me during the process of data collection, organization, analysis and interpretation.

Last but not least my family and my wife Fana for always supporting and encouragement during my study.

CONTENTS

LIST OF FIGURES

LIST OF TABLES

1. INTRODUCTION

Post-collisional potassic granitoids were emplaced in the northern part of the east African orogen, following crustal thickening (Küster and Harms, 1998). Late tectonic, post-collisional granite suites are a feature of many parts of the Late Neo-Proterozoic to Cambrian East African Orogen (EAO), where they are generally attributed to late extensional collapse of the orogen, accompanied by high heat flow and asthenospheric up rise (Küster and Harms, 1998). These post collisional granitoids intrude both juvenile Neoproterozoic crust (mainly low grade metavolcano sedimentary belts) and pre-Neoproterozoic crust (high grade gneissic terrains) and strongly reworked during the pan African episode (Küster et al., 1998).

The Arabian Nubian Shield (ANS) (Fig. 1) is dominated by supracrustal metavolcanics including volcaniclastics and immature sediments mostly metamorphosed in the green schist facies, variously deformed and intruded by granites, gabbros, and dikes. Geochemical and isotopic signatures indicate that these rocks are dominantly mantle-derived juvenile crust (Stern, 2002; Stoeser and Frost, 2006). In Ethiopia, the ANS merges with the Mozambique Belt which is the southern half of the EAO and which accommodated the most intense collision between East and West Gondwana fragments (e.g. Stern, 1994).

The shield is differentiated by the orientations of sutures, shear zones, and fold belts into northern and southern sectors: the southern shield is dominated by northerly trends; the northern sector by a variety of trends (Johnson et al., 2011). Cropping out in western Arabia and northeastern and eastern Africa, the ANS is exposed within the jurisdiction of nine nations: Jordan, Israel, Saudi Arabia, Egypt, Yemen, Sudan, Eritrea, Ethiopia, and Kenya.

The Northern metamorphic terrain of Ethiopia consists of a series of thick, inhomogeneous volcano-sedimentary assemblages that belong to the ANS of the Pan-African orogen (900---500 Ma), (Asrat et al., 2004). The ANS is a juvenile, subduction-related, accreted terrane formed by lateral crustal growth through arc---arc accretion (Kroner et al., 1987; Stern, 1994), in which mafic--- felsic plutonism played an important role (Tadesse et al., 1999; Asrat et al., 2001).

The granitoid and the volcanic assemblages are calc-alkaline and lack evidence of any Pre-Pan-African continental crust. A review of the available geochronological data (Asrat et al., 2001) suggests the existence of three periods of granitic magmatism in both the ANS and the Mozambique Belt (800---885, 700---780 and 540---660 Ma), encompassing syn-, late- and

post tectonic granites. The studied area is located in the low-grade, volcanic and volcano-sedimentary rock assemblages in western shire area (Fig. 2). It is intruded by syn-tectonic and post- tectonic granites and unconformably overlain by sedimentary rocks. Details about these granites and the geology of the studied area have been reported by (Tadesse, 1996 and 1997; Tadesse et al., 2000).

Despite the classification based on structural (deformation) and contact relationships with the country rocks to understand the granites. There is limited geochronological data constraining the age of granitic rocks and their geochemistry. We selected seven granitic samples and one metavolcanic sample from the study area (Fig. 8). The objective of this study is to carry out geological, geochronological (zircon and titanite U-Pb) and geochemical (major element, trace elements and rare earth elements) studies with the purpose of determining the geology, emplacement age of the granites, geochemistry and tectonic setting.

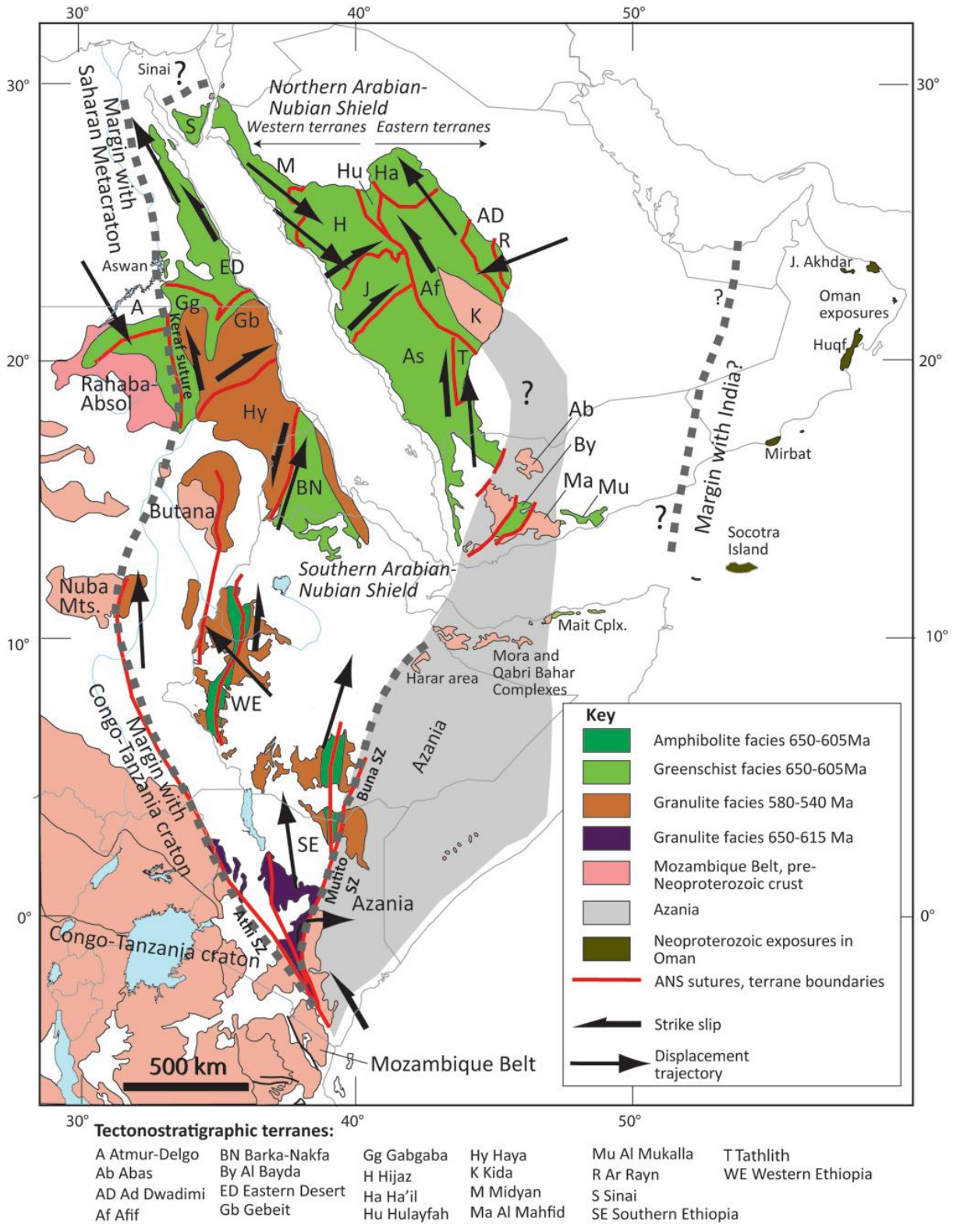

Fig. 1 Structural and metamorphic map of the ANS (from Johnson, 2014) showing tectonostratigraphic terranes, suture zones, the boundary between eastern and western arc terranes in the Arabian Shield (after Stoeser, 2006) and boundaries between the ANS and flanking older crustal blocks. Arrows show displacement trajectories and sense-of-shear during transpressive orogenic phases in the region.

2. DESCRIPTION OF THE STUDY AREA

2.1 Location and Accessibility

The study area is located about 340 km West of Tigray regional state (Mekelle), Northern Ethiopia, about 30kms West of Shire Indasillasie town. Geographically it is located between UTM of 1549000-1579000m latitudes and 380000-410000m longitudes (Fig. 2). It can be reached through the all Shire Indasillasie town-Mai Hanse all-weather roads.

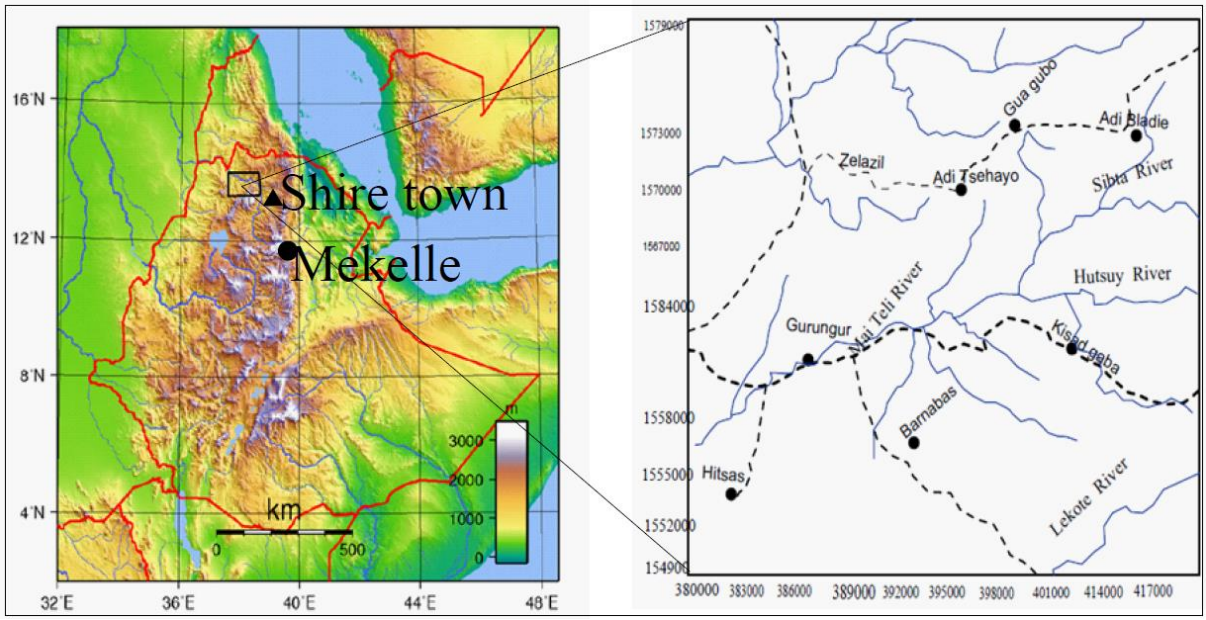

Fig. 2 Location and accessibility map of the study area (Inset rectangle) shire town (black triangle), Mekelle city (circle) in northern Ethiopia

2.2 Physiography and climate

The study area is characterized by rugged topographic terrains in the south west, north east, northern most parts and flat topography at the central part. The metavolcanic, ultramafic, and the granites occupy the mountainous ridges and the metasedimentary rocks occupy the flat areas.

The northern, western and southeastern parts of the area are rugged mountains underlain by Precambrian metamorphic and intrusive rocks. The southern and eastern parts of the area have gentle, undulating and dissected topography and are characterized by flat topographic feature.

The climate of the area is characterized by semiarid to arid conditions, with hot tropical climate. The two main rainy periods are June to mid-September with intermittent rains during

March. The average annual rain fall is 600 to 800 mm and the mean annual rain fall is 632.5 mm.

The annual average temperature of the area reaches about 38^0c during the day time and at night 18^0c in the dry season; and in the wet season 25^0c during the day time and 8^0c at night. The mean maximum, mean minimum and mean annual temperature is 30.2^0c and 16.4^0c respectively (Ethiopian Metrological Service Agency, 2012).

The prevailing vegetation of the area is very scarce and devoid of vegetation at some places. The vegetated areas are covered by thorny bushes, scattered tress, long savanna grass grown during the rainy season and incense trees are also available. There are also all season vegetation in the mountainous terrains of the area.

The drainage system of the area is defined by dendritic pattern and the various streams slops to the south west. The streams and rivers of the area are dry and some are intermittent.

2.3 Human settlement and land use

The area is inhabited by subsistence farmers and sparsely populated and population density vary from place to place. The people subsist mainly on rain-fed agriculture cultivated in the area. Cultivation Sorghum, maize and millet are the most widely practiced and other fruit trees are being developed. Livestock breeding is also practiced in conjunction with cultivation of cereals. Panning of the delluvium and alluvial gravels and for gold is being practiced by the local people as a means of obtaining additional income. Artisanal mining activities were recovering placer gold by panning, which are generating substantial income for the local community.

The villages in the area are sources of relatively cheap labor. The availability of labor is usually seasonal. During the dry seasons, labor is relatively abundant, whereas there might be relative decrease of the available labor force during the rainy season (June to September) and during the harvest time (October and November). Generally, the people live in scattered settlements. Most of the settlements are concentrated in the Kisad Gaba, Hitsas, Mekayeho, Waelo and Sibta villages.

3. GEOLOGICAL SETTING

3.1. Geodynamic evolution of the East African Orogen

The EAO developed due to the collision of East and West Gondwana (Fig. 3) during the late Proterozoic, which finally formed the Gondwana Supercontinent (de Wit and Chewaka 1981; Stern 1994; Stern 2002; Stern et al. 2005). The EAO also represents one of Earth's greatest collision zones. This orogen is about 6000km long and evolved over a time period of about 350 Ma (Stern, 2002).

The tectonic evolution of the EAO is: (1) Rodinia rifting and break-up at ~900-850 Ma; (2) seafloor spreading, arc and back-arc basin formation, and terrane accretion from 870 to 690 Ma; (3) continent-continent collision from 630 to 600 Ma, and (4) further crustal shortening, orogenic collapse and extension leading to the break-up of Gondwana during 600 to 540 Ma (de Wit and Chewaka 1981; Stern 1994; Stern et al. 2006).

The southern part of the EAO is represented by the Mozambique Belt, which was formed by a Himalayan-type collision. The Mozambique Belt comprises high-grade gneisses, migmatites and schists (Asrat et al. 2001). This belt can be traced in southern, western, and eastern Ethiopia (Berhe 1990; Asrat et al. 2001).

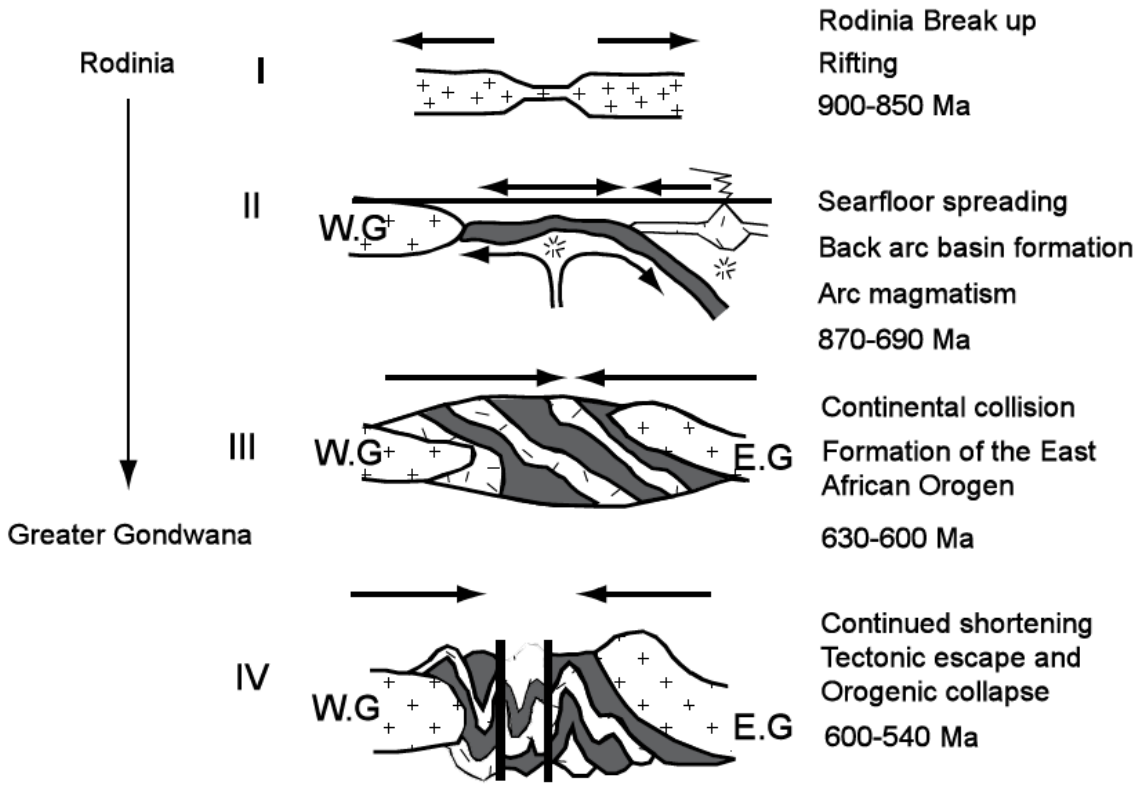

Fig. 3 Tectonic evolution of the East African Orogen that resulted in the greater Gondwana Super continent (Stern et al., 2006). W.G=West Gondwana and E.G=East Gondwana.

3.1.1 Geology of the Arabian-Nubian Shield

The ANS is the northern half of the great collision zone called the East African Orogen (Fig. 1) which is formed at the end of Neoproterozoic time when east and west Gondwana collided to form the supercontinent Gondwana (Vail, 1985; Stoeser and Camp, 1985 Johnson, 2011 and 2014). It mainly consists of sutured low grade assemblages of Neoproterozoic volcanic, volcano sedimentary and sedimentary units, intrusives and contains many remnants of oceanic crust in the form of ophiolites (Abdesalam and Stern, 1996; Tadesse, 1996; Alemu, 1998). It extends 2200 km along north-south and 1200 km east-west and is represented by Precambrian crystalline rocks, exposed along the flanks of the red sea.

Many studies and publications have already been documented on ANS particularly of the Arabian side of the shield with integrated approaches of radiometric, isotopic and geochemical investigations. Some of these studies have showed the progressive change in chemistry of arc-magmatism with time of cratonization process basically from early (>900Ma) primitive, low K, are tholeiite to late (700-600Ma) evolved, high K, calc-alkaline lava series (Roobol et al., 1983; Stoeser and Camp, 1985).

According to the deformation belt, (Abdelsalam and Stern, 1996) have divided the ANS into two deformation belts: (1) Related to arc-arc and arc-continent collisions, which are both associated with sutures. The arc-arc deformation belts are manifested by the occurrence of E-W and N-S verging ophiolities in the northern and southern parts of the ANS, respectively (Abdelsalam and Stern, 1996). The E-W verging ophiolities are steepened by upright folds, whereas those of N-S vergence are deformed by up-right folds and Strike slip faults related to oblique collision of the terranes at about 800-700 Ma (Abdelsalam and Stern, 1996). The arc-continent deformation belts are related to the collision of East and West Gondwana. (2) Post accretionary structures (~650-550 Ma) resulted from continuous shortening of the ANS and developed NW trending strike slip faults and shear zones during the waning stages of ANS formation. It has been early since the northern Eritrea has considered as part of the ANS right after the definition of Tokar Terrane, volcano sedimentary and plutonic assemblages exposed east of the Barka suture in Northern Eritrea and South eastern Sudan, which was correlated to the Red Sea and south western part of the Asir Terrane of Saudi Arabia. Further advanced studies using field data and remote sensing imageries have showed the complexity of this terrain (Tokar terrain) and hence led to the further division of the Eritrean basement into different Proterozoic terrains trending north to northeast with better explanation of their development in the context of accretionary tectonics (Abdelsalam and Stern, 1996).

In Eritrea, the Neoproterozoic basement rocks have been divided into four terranes on the basis of distinct stratigraphic and structural characteristics, (Barrie et.al.,2007) including: the Barka terrane to the far west (predominantly amphibolite-grade metasedimentary and mafic gneisses), the Hagar terrane to the north (principally mafic metavolcanic rocks, including ophiolite-like assemblages), the Arig terrane and the Nakfa terrane, the largest of the four (granitoid-greenstone belts and syn to post-tectonic granitoid rocks), and to the east (granitoid and metasedimentary). Almost all of the volcanic-sedimentary rocks of the Nakfa terrane strike north-south (±25 degrees), and there is a significant volume of syn- to post-tectonic granite between the western and eastern halves (Barrie et. al., 2007). It has generally believed that the Nakfa Terrane of the Eritrean basement has served as a linking terrane which connected the geology of northern Ethiopia particularly of Axum area to the rest of ANS in the north.

3.1.2 Geology of the Ethiopian basement rocks

The Ethiopian basement rocks are exposed in eastern, western, northern, and southern parts of the country (Fig. 4). They have been studied for the last three decades by researchers such as (Kazmin, 1971, 1975; Kazmin et al., 1978; Beyth, 1972a; de Wit and Chewaka, 1981; Ayalew et al., 1990; Alemu, 1998; Tadesse, 1996; Tadesse et al., 1997, 1999, 2000; Alene et al., 2000, 2006; and Asrat et al., 2001).

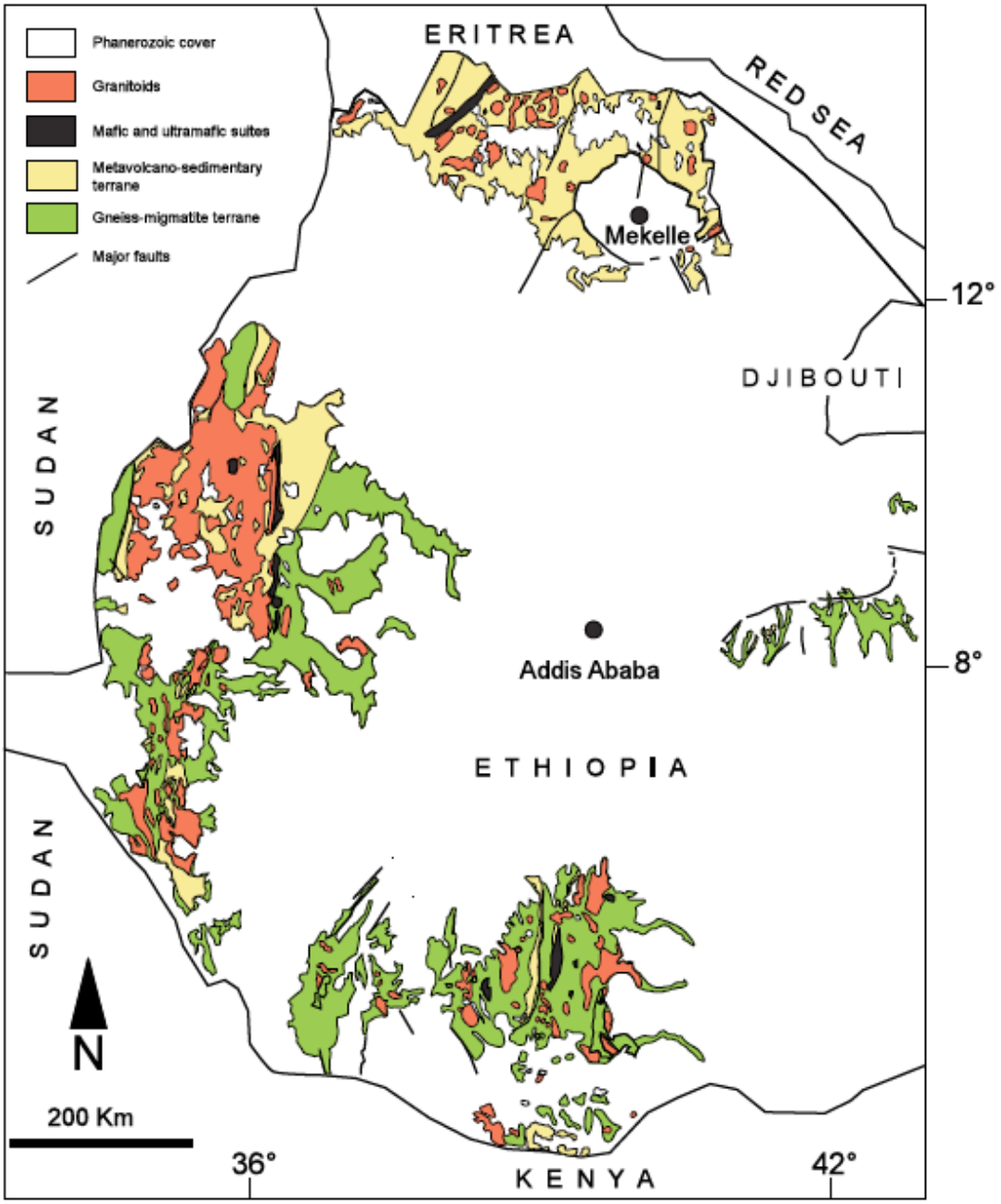

Fig. 4 Distribution of Ethiopian basement rocks (Gebresilassie, 2009)

(Kazmin, 1971, 1975), who explored the basement rocks for the first time subdivided them into Lower, Middle, and Upper Complexes based on compositional, deformational and metamorphic grade variations. Recently, this subdivision has been revised as the rocks of Lower Complex, which was thought to be Archean in age, turned out to be Late Proterozoic in age (e.g. Ayalew et al., 1990; Teklay et al., 1998). According to the new subdivision, the Ethiopian basement is composed of two major blocks: (i) a gneissic and magmatic terrain, which essentially consists of the Lower and Middle Complex (Kazmin, 1971, 1975), and

correlated with the Mozambique Belt; (ii) a low-grade volcano-sedimentary terrain, which comprises all the rocks of the Upper Complex and is correlated with the ANS (Fig. 4). Pre-, syn-, and post-tectonic granitoids intruded the Ethiopian basement rocks (Asrat et al., 2001).

3.1.3 Geology of Tigray basement rocks (northern Ethiopia)

A detailed classification of the basement rocks in northern Ethiopia has been made by (Gass, 1981; Kroner, 1985; and Shackleton, 1986). According to these researchers, the Neoproterozoic sequence of Tigray forms the southern end of the ANS. In Tigray, low-grade, meta-volcanic, meta-volcanoclastic, and meta-sedimentary rocks are intruded by syn- to late-tectonic granitoids (Beyth, 1972a and b; Kazmin et al., 1978; Tadesse, 1996; Alene, 1998; Tadesse, 2000), the meta-volcanic and meta-volcanoclastic rocks together forming the largest unit.

The green-schist facies represents the volcano-sedimentary sequences in the northern Ethiopia. The Axum sheet of northern Ethiopia provides an insight into the geology of northern Ethiopia which is part and a reflection of the ANS (Tadesse et al., 1999). This work on geochemistry of low grade metavolcanic rocks from the Pan-African of the Axum area has demonstrated the presence of accreted intra-oceanic arc sequences with varied lithological and geochemical characteristics (Tadesse et al., 1999). This study has also showed strong consistency with studies conducted on Eritrean basement. Hence, the extension of the Pan-African ANS further to south in northern Ethiopia has become evident. Accordingly, six tectonic bounded and north to north east trending tectonostratigraphic sequences were identified including; the Shiraro, Adi Hageray, Adi Nebrid, Chila, Adwa and Mai Kenetal blocks. The geology of each block was summarized in (Tadesse et al., 1999). It has generally believed that the Nakfa Terrane of the Eritrean basement has served as a linking terrane which connected the geology of northern Ethiopia particularly of Axum area (including the research area) to the rest of ANS in the north, mainly for two reasons. The first reason accounts for the spatial extent of the terrane and its spatial association with Axum area (Tadesse et al.,1999) and the second reason accounts due to their gross lithological and structural similarities as reported by(Howe,2009, 2011). The general geological history and sequence of geological events of the region have been summarized as follows; (1) deposition of volcanic and sediments underwater marine condition followed by Pan-African metamorphic event mainly of green-schist regional metamorphism (2) accretion of Proterozoic meta volcanic and meta

sediments (3) intrusions of granitic intrusives of Pan-African age (4) deposition of phanerozoic sediments (5) uplift and eruption of basaltic lava. The Neoproterozoic assemblage of the Tigray region consists of two groups the oldest being the meta-volcanic/meta-volcanoclastic unit (also called the Tsaliet Group), followed by phyllite, slate, and carbonate, which fall under the Tambien Group, and the syn- to post-tectonic plutonic units, granite to granodioritic composition (Tadesse et al., 2000; Asrat et al., 2001; Alene et al.,2006), (Fig. 5).

3.1.3.1 Tsaliet Group

The late Proterozoic Tsaliet group is well constrained in the Tigray region and covers major part of the region. The Tsaliet group consists of calc-alkaline, island arc related metavolcano-sedimentary rocks including metavolcanic/volcanoclastic rocks, sericite-chlorite schist, slate, grey wacke, impure marble, calcareous siltstone, well bedded, intermediate to acidic welded tuffs, lappili tuff, and agglomerates (Beyth, 1972; Beyth et al., 2003; Tadesse et al., 1999; Alene et al., 2000).

The rocks are green to purple schist containing stringers of quartz, epidote and calcite, interbedded with black, white, green and pink quartzite; pink to light green gneiss, and minor black limestone and light green marble. Green schist originally well bedded agglomerate and tuff, quartz schist originally rhyolitic volcanics, well bedded, with graded bedding and ripple marks. Its thickness reaches up to 1500 meters and is unconformably overlain by the Tambien group (Beyth, 1972). The NE-SW trending shear – zones with a sinistral – strike slip displacements affect the rocks of Tsaliet Group (Tadesse et al., 1999). This predominantly volcanic sequence merges into the overlying Tambien group.

3.1.3.2 Tambien Group

The Tambien group is a 2-3 km thick silciclastic-carbonate succession overlying the Tsaliet group (Fig. 6). It was developed in intra-oceanic arc platform setting, southern extension of the Nakfa terrane in Eritrea. The Tambien Group was deposited in a shallow marine environment during a period of regional arc-magmatic lull (Avigad et al., 2007). This is mainly exposed in a series of synclinal inliers surrounded by the Tsaliet Group rocks.

The main rock units in this group are slate, phyllite, graphitic schist and metalimestone.

This group is further subdivided from the oldest to the youngest, into Weri Slate (which contains black to blue – greenish, well laminated and foliated slate, greenish calcareous slate,

and black silty greywacke at some places it grades into phyllite and graphite schist); Assem Limestone (medium to finely crystalline, well bedded and fragmented containing silicified lenses and dolomite at base. The rocks are well lineated parallel to strike of bedding.); Tsedia Slate (green-grey to black slate, graphitic in part, well laminated and interbedded with fine grained calcareous sandstone and purple slates at the base of the section. The units are intruded by aplitic dikes.); and Maikenetal Limestone (it is black, finely crystalline, well bedded with detrital algae fragments, ooliths and rare plagioclase crystals cut by quartz veins. This unit is well lineated parallel to strike of bedding (Beyth, 1972). The Tambien Group was deposited in a shallow marine environment during a period of regional arc-magmatic lull (Avigad et al. 2007).

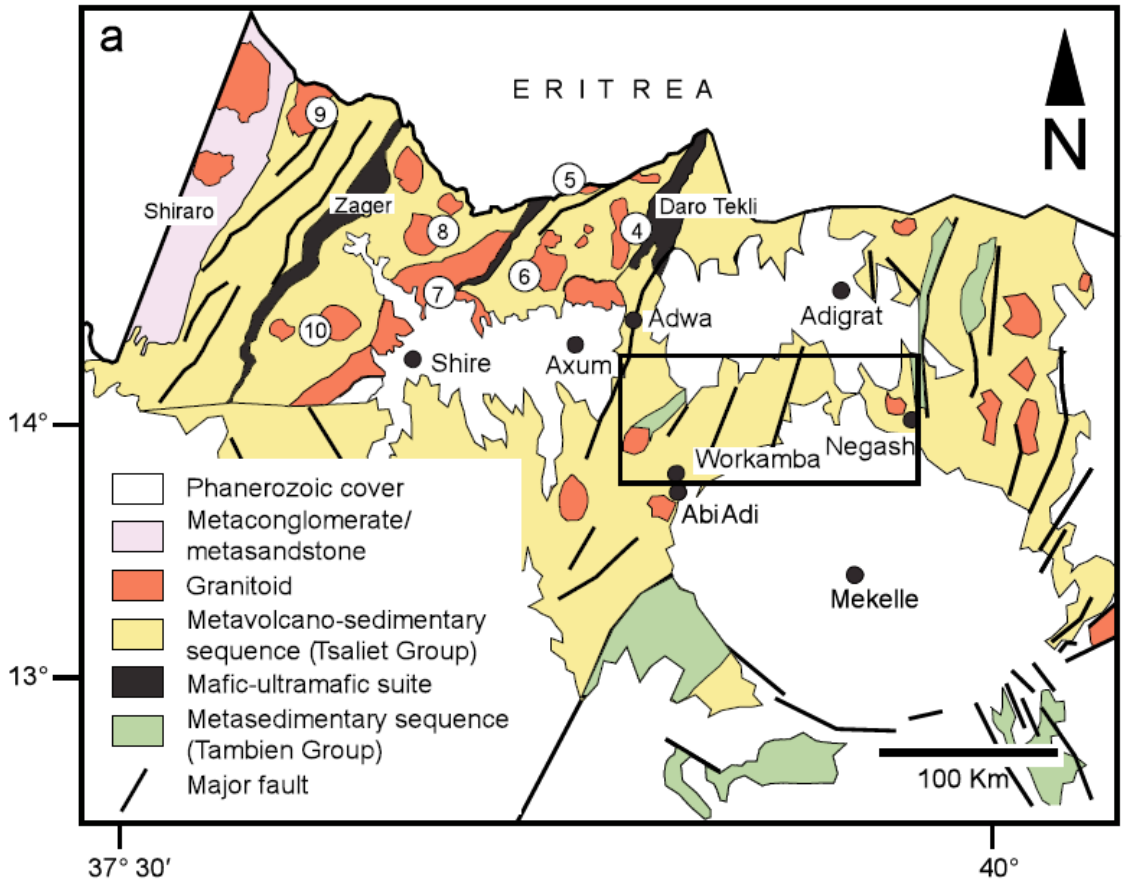

Fig. 5 Distribution of the Tsaliet and Tembien group rocks in the Tigray region,northern Ethiopia (from Gebreslassie, 2009). The circles with number represent the location of dated granitoids in the region, which are both syn- and post-tectonic in origin (1= Negash, 2 = Hawzen, 3 = Mai Kenetal, 4 = Rama, 5 = Mereb, 6 = Chila, 7 = Shire, 8 = Deset, 9 = Azeho, and 10 = Sibta granitoids).

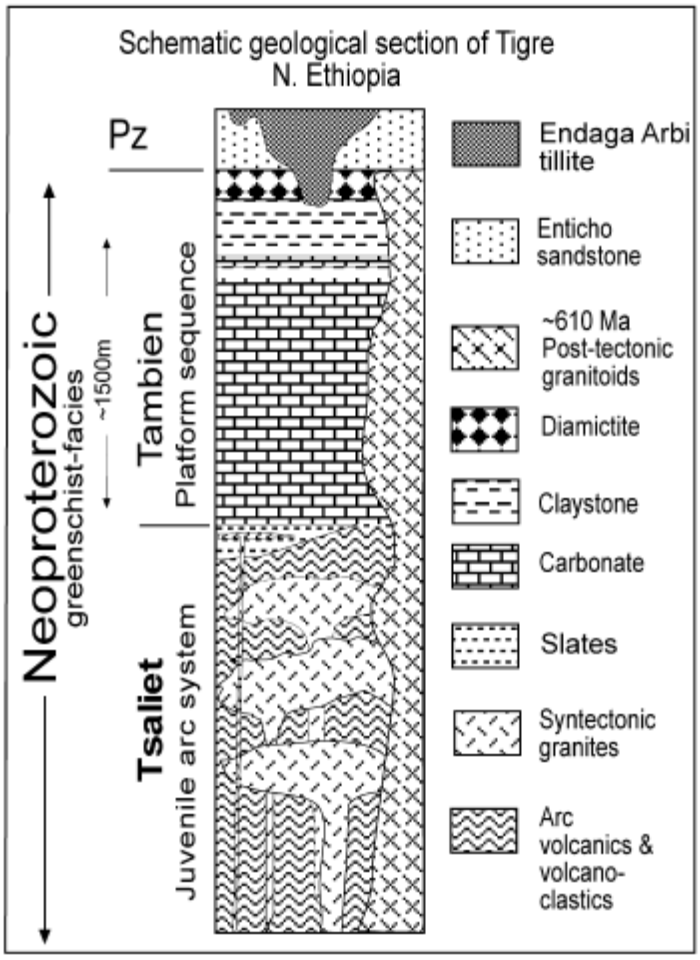

Fig. 6 Schematic geologic columnar section of Tigray region showing main rock units (From Avigad et al., 2007). Two major Neoproterozoic units are distinguished: Tsaliet Group (metamorphosed arc volcanics and syntectonic granitoid intrusions) and overlying metasediments of the Tambien Group. Diamictites comprise the top of the Tambien Group. The entire Neoproterozoic section is pierced by post-tectonic Mereb-type granitoids. Ordovician (Enticho) sandstone and associated Endaga Arbi tillites overly the peneplained basement.

3.1.3.3 Geological structures of Tigray with reference to ANS

The major structural feature in the northern Ethiopia is the northeast-southwest striking and variably southeast and northwest dipping composite foliation (Tadesse, 1996).

The Precambrian rocks have experienced different phases of deformation. The tectonic structures include the fold-thrust domains with associated shear zones of predominant sinistral sense of shear which are attributed to major collision orogeny during the amalgamation of the

ANS (Tadesse et al., 1999). In addition, the study area as part of the Adi Nebrid block, structurally characterized by the presence of series of anticlines and synclines, wide spread shear zone trending NE-SW with sinistral slip movement and thrusting with NW vergence in contact with Zager mafic/ultramafic intrusive (Tadesse et al., 1999).

The study area was affected by five phases of deformation as described by (Tadesse, 1997).

The first phase of deformation (D1) in the Asgede domain of the block has produced S1 fabric. This fabric is transposed metamorphic layering in fine grained phyllitic and graphitic schist. In these rocks, the intercalated thin competent quartzitic layers are strongly disrupted and preserved as thin elliptical lenses or rootless, intrafolial F1 folds. These F1 folds are generally isoclinals, have strongly attenuated limbs and rounded hinge zones. Similarly, due to the transposition during the D1 event, graphite stripping in phyllitic schist and vise versa are common. Strongly developed lepidonematoblastic texture, defined by chlorite and actinolite minerals in metavolcanics are also the product of this phase of deformation. The S1 fabric is axial planar to the fold.

The second phase of deformation is upright to gently inclined major antiformal and synformal structures. The S1 fabrics are folded around these major F2 folds. Mesoscopic F2 folds are scarce. The observed F2 mesoscale folds are disharmonic crenulations and occur along the hinge zones of the major F2 folds. S2 is represented by spaced, fracture cleavages and cut the S1 fabric at high angle.

The third phase of deformation in the domain is a ductile shear zone, confined to the contact zone of granitoids. Steeply dipping S3 mylonitic fabric is developed in either side of the intrusive bodies. Asymmetric structures, S-C fabrics (Berth et al., 1979), rotated σ structures (Simpsons and Schmid, 1983), steeply plunging asymmetric mesoscopic folds (Bell, 1981), horizontally plunging mineral aggregate and elongation lineation in the shear zone, invariably indicate a sinistral strike slip sense of movement during the D3 deformation in this sub domain.

The fourth phase of deformation consists of N-S striking and vertically dipping brittle-ductile shear zones transacting the generally NE-SW structural grains. The rocks in the shear zones are strongly silicified. Quartz veins are common following the shear belts. Kinematic indicators area not well developed. However, some shifts in the contacts of stratigraphic units across the shear zone indicate sinistral sense of displacement.

The last phases of deformations are the WNW-ESE faults with dextral sense of displacement joints of variable orientation are categorized under this phase of deformation.

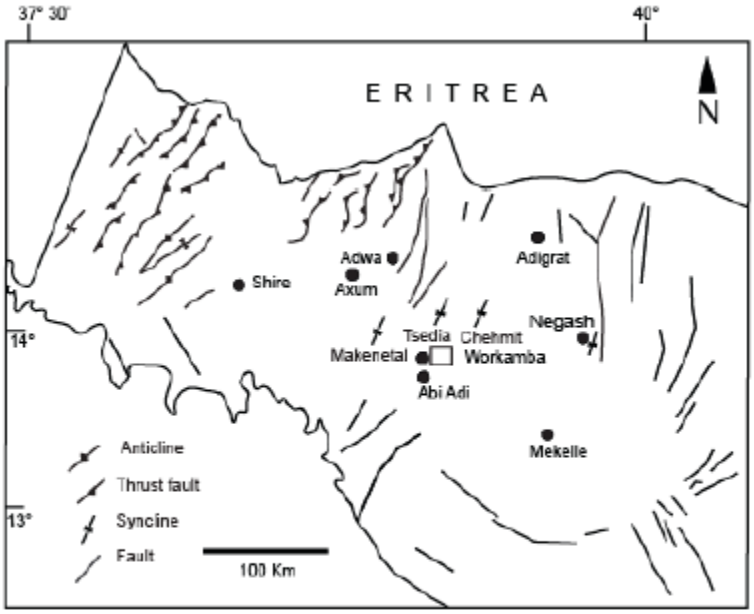

Fig. 7 Distribution of major tectonic structures in Tigray (From Gebreslassie, 2009).

3.2 Geology of the study area

The study area constitutes Precambrian basement terrane, which in turn is classified further into Tsaliet and Tambien groups are well exposed. It consists of mainly metavolcanics, sericite quartz-feldspar schist, phyllitic and graphitic schist, mafic –ultramafic rocks, sedimentary rocks and Granites (Fig. 8). The main lithologies are intruded by syn-to late tectonic granites.

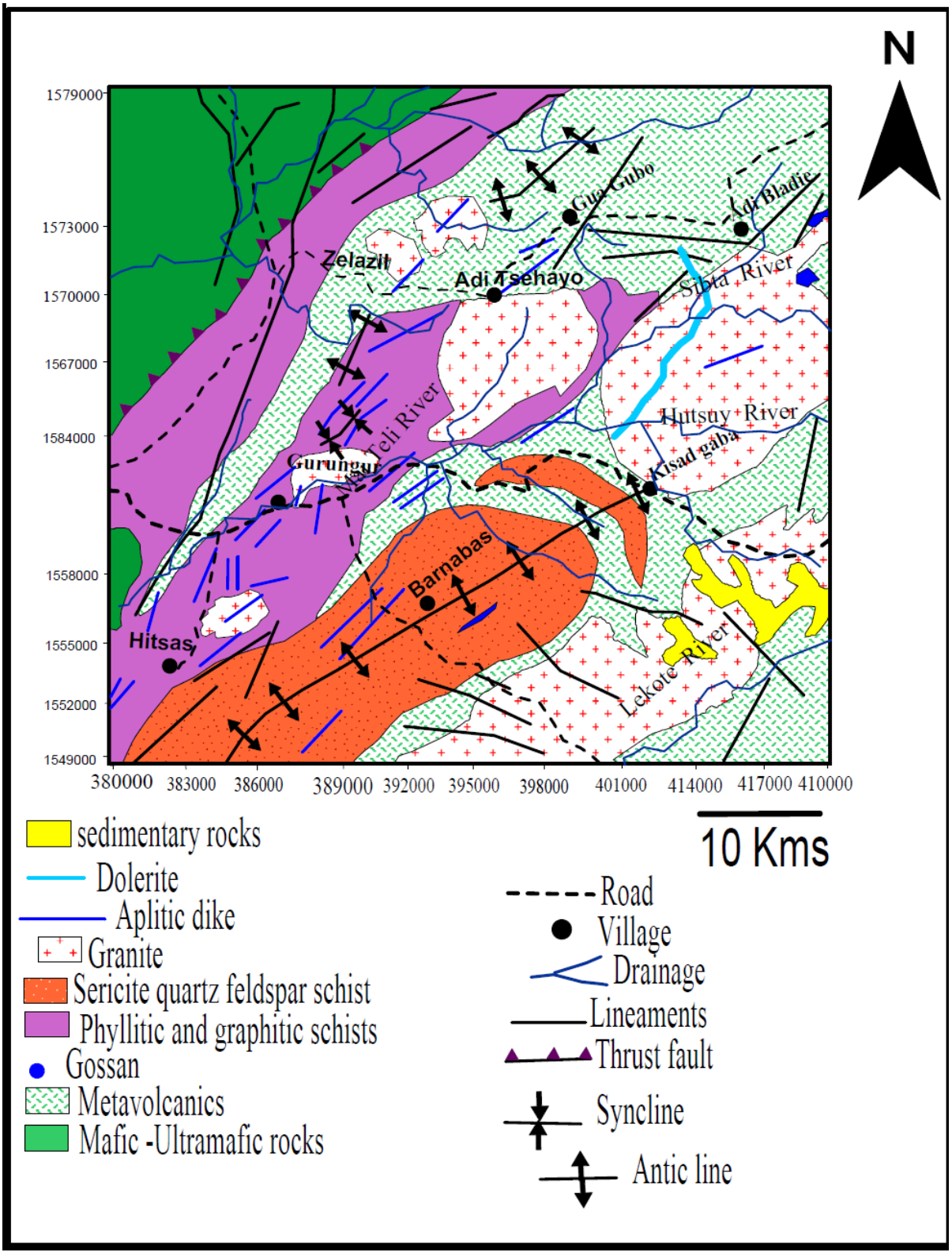

Fig. 8 Geological map of the study area (After Harvest, 2010; Tadesse, 1997)

3.2.1 Mafic- ultramafic rocks

The ultramafic unit of the area is regionally correlated to the Zager mafic ultramafic belt (i.e. northwest of the study area). It is bound by a thin zone of carbonate metasediment on the southeast and meta-agglomerate on the northwest. They are sheared and brecciated at the contact zone between the adjacent units, marked by tectonic thrust faults and steep shear zones (Fig. 8).

It is mainly composed of chlorite, talc, serpentine, pyroxene, and amphibole porphyroblasts. It is associated with gabbro, feldspar chlorite-schists assemblages and basic metavolcanics. The chlorite schist contains disseminated magnetite probably suggesting a post tectonic mineralization.

3.2.2 Metavolcanic rocks

The metavolcanic rocks consist of basic metavolcanic, intermediate metavolcanic, and felsic metavolcanic rocks. These rocks show a gradational change of basic to felsic metavolcanic flows, locally with metavolcanic clasts. The study area is mostly covered by metavolcanic rocks.

The basic metavolcanic rock is greenish, fine grained and massive consisting of traces of quartz and feldspar. It outcrops largely in the northeastern portion of the research area. The unit in the central part is intruded by the granites. In the southern and southwestern extension area it is largely overlain by the meta-carbonates and sericite quartz feldspar schist in an antiform at Barnabas. The mafic flows and pyroclastics occur as layered, lensoid massive bodies bearing in-situ brecciation. These are closely associated with pyroclastics containing fragments of amphibole porphyry.

The common alterations were sericitization, sulfidation and carbonatization. Carbonatization is more pronounced in the mafic volcanics whereas the remaining alterations have pervasively altered the phyllitic and graphitic schists. Most of the volcanogenic massive sulphides so far identified in Adi Bladie area are found hosted within the mafic and felsic metavolcanics close to the contact with granite.

The felsic metavolcanics are fine grained glassy texture and vary in color from greenish grey to light grey. The felsic metavolcanics also display variegated colors, brown to pale-grey. The felsic metavolcanic is composed of mainly quartz, feldspar and sericitization and kaolinitic alterations. The rock is intensively intruded by quartz veins having different

orientation and thicknesses ranging from 5 to 20 cm. During the field work we encountered porphyritic metarhyolite dikes with blue quartz eyes.

3.2.3 Phyllitic and Graphitic schists

The phyllitic and graphitic schist consists of various units derived from volcanoclastic and mafic flows. It is dominantly composed of graphitic phyllite, graphitic slate, quartzite and metagreywacke. It is intruded by granites at the central and northeastern of the syncline. They are dark grey colored, fine grained, highly foliated, composed of graphite, micas (dominantly muscovite), and minor amount of fine grained chlorite, feldspar and quartz. Massive gossan with old malachite excavation along the crest of Hitsats ridge were observed. Along the ridge to the southwest of the massive gossan, quartz veins with high grade gold are reported (personal communication). On the southeastern foot of the ridge the local people pan gold from the alluvium and delluvium. From the geomorphologic, structural and compositional point of view, the metasediments were deposited above the meta-volcanic rocks in a reducing sub- marine geosynclinal environment.

3.2.4 Sericite quartz feldspar schist

This is exposed along the central part of the Barnabas anticline in contact with the felsic-mafic metavolcanic rocks to the east and graphitic schist western part of the research area.
It is moderately oxidized, chloritized, sericitized, and locally silicified with grey to pale yellow color and fine grained in texture (Fig. 9). The phyllite and graphite schist are encountered as intercalation within this lithology.
This is among the major litho-strata in the study area and is exposed at the central part of the antiform having a length of approximately about 10-20 km in the northeast-southwest direction. This is constituted by Sericite- quartz- feldspar schist with thin layers of metarhyolite, and minor felsic-mafic metavolcanics. These rocks are horizontally to sub-horizontally layered dipping 45^0northwest and southeast along the hinge zone. At the western and eastern margin the anticline (i.e. along both sides folded limbs) the layers are relatively steep between 60^0 to 65^0 northwest and southeast. The northeastern closure of the fold, the strike of the foliation varies from northeast to northwest and dips 35^0 to 45^0 to the northeast.

Fig. 9 Sericite quartz feldspar schist southern Kisad Gaba

3.2.5 Intrusive bodies of the study area

The study area exposes various types of granites with several aplitic dikes, dolerite dikes, pegmatitic veins and quartz veins.

The granites show wide variation in texture from fine-medium to coarse grained and a similar mineral assemblages and foliation in individual granites were observed.

These include the Kisad Gaba granite, Gurungur granite, Adi-Tsehayo granite, Zelazil granite, and Hitsas granite.

The granite outcrops are represented by well-rounded boulders and in some places vary in shape from elliptical to subrounded and with parallel arrays of elongated exposures. Two distinct types of granites were identified; grey or pale and pink (red) that belong to the same felsic magmatic phase exposed. The individual granites details are given below.

3.2.5.1 Hitsas granite

This granite is exposed at the south-western part of the study area occupying low lying gentle topography covering less than 1 km^2 in and around Hitsas town. It is hard, compact, fine to medium grained, massive and at some places porphyritic in nature and light grey to dark grey in colour. It is dissected by various joints and exfoliation fractures producing rounded massive blocks.

The constituent minerals are quartz, alkali feldspar, plagioclase, and biotite. The Hitsas granite is rounded to elliptically shaped and intensively intruded by dikes. The Hitsas granite is also characterized by the presence of xenoliths and contact baking effect were also observed on surface exposures. In places, the granite is dominated by large elongated K-feldspar crystals.

The granite is locally foliated, and mildly deformed. Most of the granite shows variation in composition from granitic to slightly intermediate granodiorite.

The granite intrudes discordantly graphitic schists and phyllites. Although not evident in the map and local blocks and small exposures suggest that the granite continues in a northern direction towards the Gurungur area.

The granite is also traversed by intensive and randomly oriented aplitic dike and pegmatite trending E-W defined by the parallel alignment of the micas, quartz and elongated feldspars crystals.

It is silicified, weathered and fractured. Folded pegmatite veins are common along the contact of the granite. The pegmatite veins are mainly exposed in central part of the Hitsas granite. The pegmatite is coarser than the surrounding granites. There are also quartz veins and local people are engaged in gold panning from the soil in their immediate vicinity.

Three representative samples were collected for chemical analysis and thin sections and one sample for dating from the Hitsas granite.

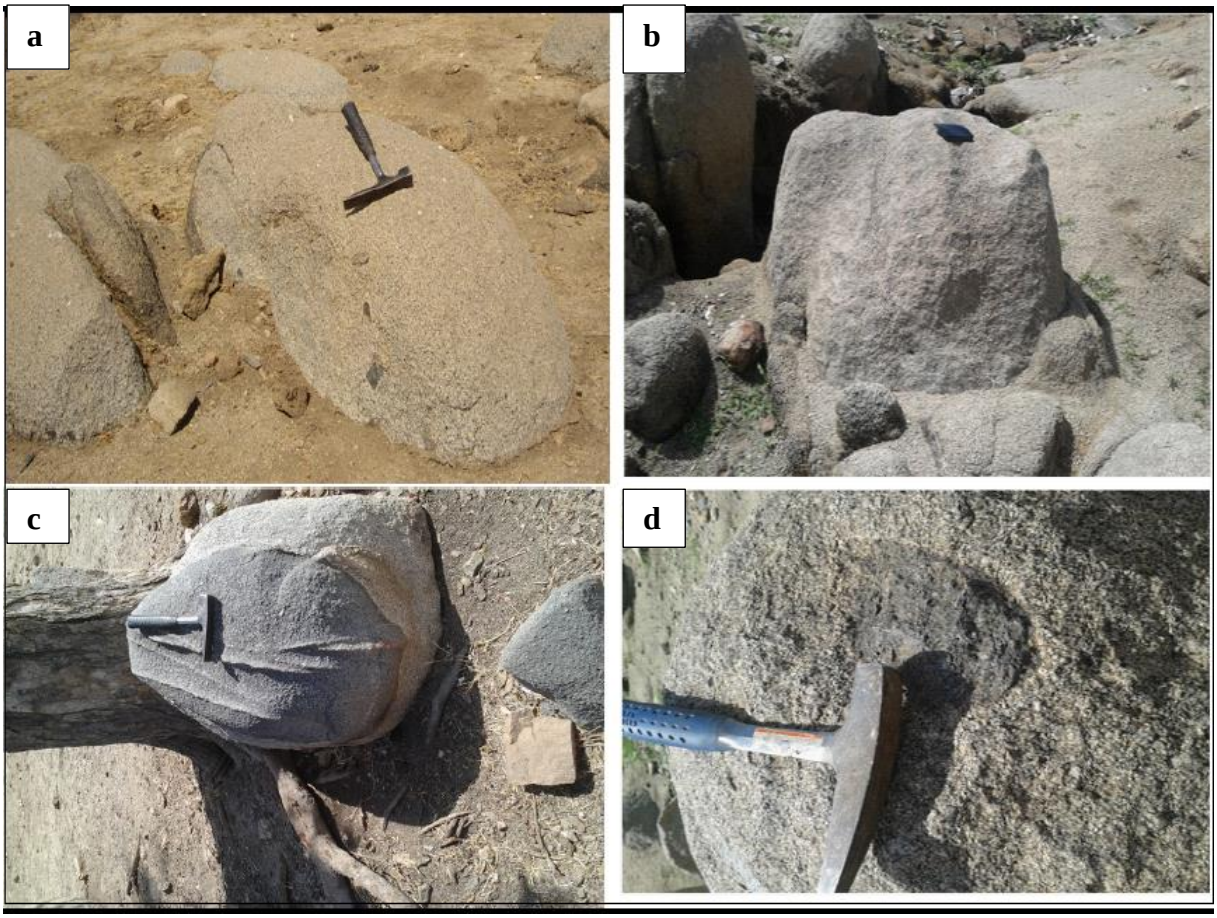

Fig. 10: Field characteristics of Hitsas granite and enclaves **(a)** elongated boulder type with dark rectangular xenoliths, (b) typical style of exfoliation weathering (c) contact baking effect /in central part of Hitsas village and (d) rounded shape dark xenoliths

3.2.5.2 Gurungur granite

The Gurungur granite is exposed in the south-western part of the study area forming a rugged topography dissected by joints (Fig. 11 a, b). It is light grey to pink colored, fine grained and occurs as large blocks. It is composed of plagioclase, K-feldspar, quartz, and biotite,. The granite is also well exposed along the Mai Teli River.

This is also characterized by narrow contact zone and with fabric development.

The Gurungur granite is associated with late magmatic aplitic dikes, which are fine to meduim grained and fractured, and pegmatitic dikes. These aplitic and pegmatitic dikes cut the granitic intrusive body. The aplitic dikes continue south ward across the Mai-Teli river having a NE-SW elongated shape. The same K-feldspars are exposed inside and outside of the mafic enclaves (Fig. 11c).

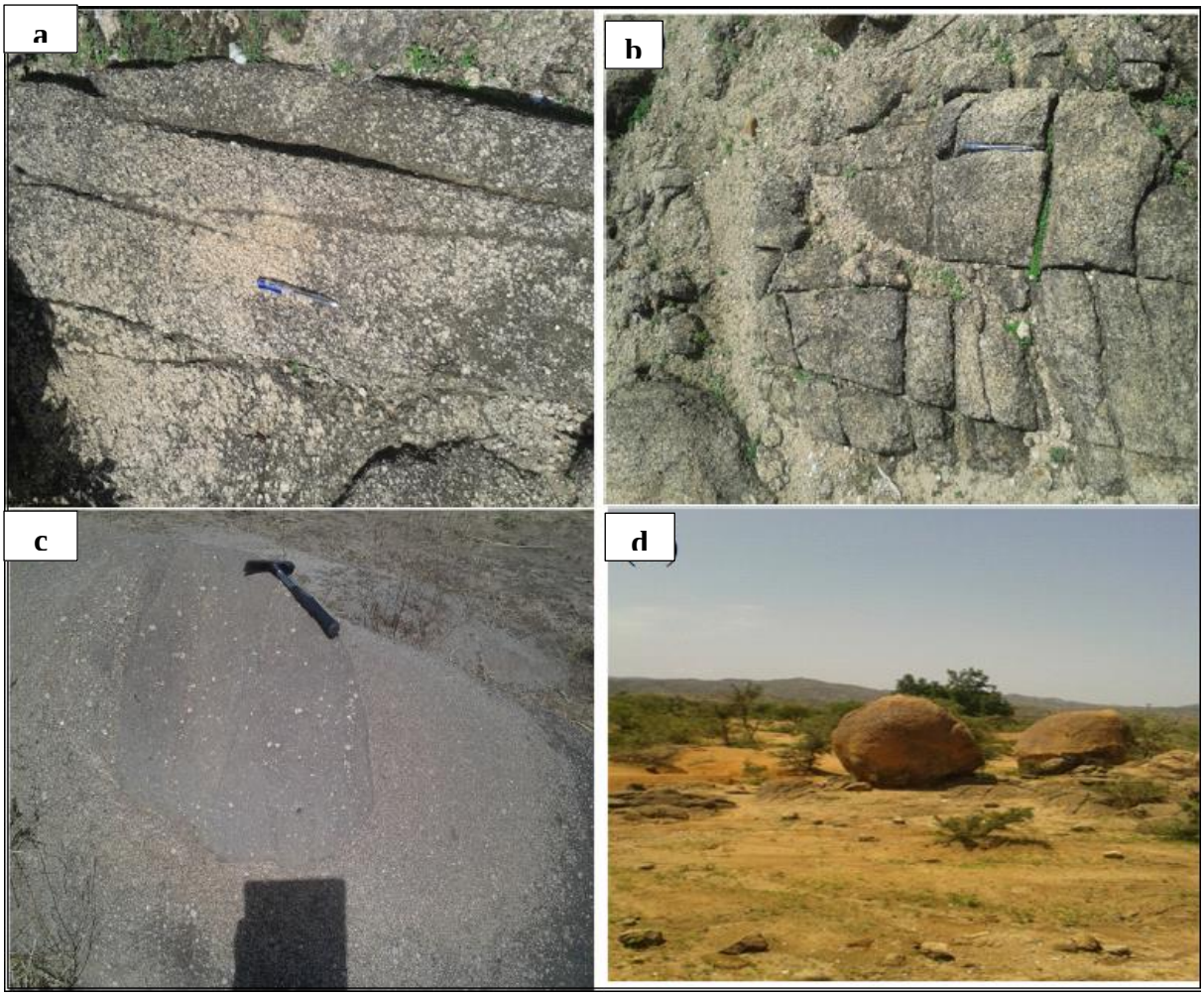

Fig. 11: Field characteristics of enclaves, joint fractures of Gurungur granite

(a), (b) fractured with joint sets and weathered granite, (c) Elongated creamy k-feldspar phenocrysts same in and outside of the enclave, (d) boulder type granite in Gurungur area

3.2.5.3 Kisad Gaba granite

This granite outcrops in and around Kisad Gaba village covering an area of greater than 10 km^2. The granite is characterized by a subrounded to elongated shape occupying relatively rugged topography, mountains and along both sides of the Hutsuy River.

In some places, the granite is characterized by semicircular, elliptical in shape, intruding the metavolcanics and metasediments. The granite is pinkish to reddish in color, coarse grained, granular and constituted by minerals of K-feldspar, plagioclase, quartz, muscovite, and biotite.

It shows a porphyritic appearance owing to the presence of randomly oriented K-feldspar phenocrysts.

The granite is massive and undeformed and appears to cut the Barnabas anticline. There quartz veins, dolerite dikes (Fig. 8) cutting the whole granite at the center and shears developed within the metavolcanics and phyllitic –graphitic schist trending in a NE-SW orientation which is consistent with the regional structures. The quartz veins, dolerite dyke and pegmatite veins are cut the granite discordantly.

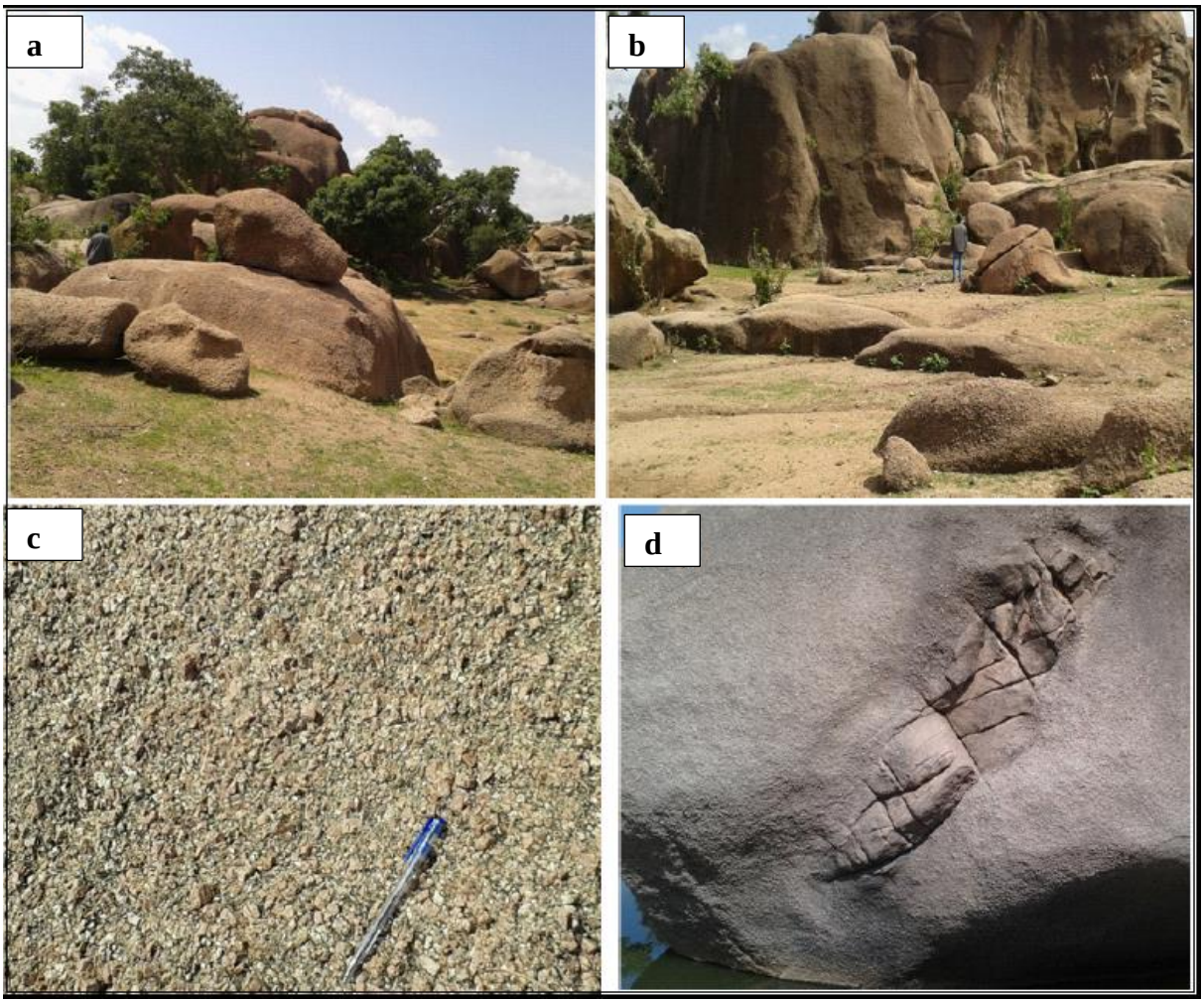

Fig. 12: Field characteristics of the granite at north of Kisad Gaba village **(**a) and (b) large and elongated blocks, (c) grey-pink porphyritic texture with K-feldspar crystals, (d) fractured aplitic dike mingled with porphyritic granite at north of Kisad Gaba village

3.2.5.4 Adi Tsehayo granite

This granite unit is exposed in the northwest part of the study area occupying a flat to rugged topography covering approximately 6 km^2. It is light grey to pink colored, characterized by coarse grained pink and porphyritic to pegmatitic textures. The granite occurs as sub circular to elliptical, blocky and it contains porphyritic phenocrysts of K-feldspars and can be monzodiorite in composition.

Along the northern margin of the granite adjacent with phyllitic-graphitic schist rocks, there is a lineament trending NE-SW that might suggests clear impact on the emplacement of Adi Tsehayo granite. This granite has no well exposed contact with the felsic to mafic metavolcanic and phyllitic to graphitic- schist. Carbonate metasediment were observed close to Adi- Tsehayo granite near the anticline and syncline.

3.2.5.5 Zelazil granite

The Zelazil granite comprises two separate bodies in the northwest of the map, intruding the felsic –mafic metavolcanics. It is exposed in a flat to gentle topography covering about 3-4.5 km^2. It has a porphyritic texture due to the presence of laths of K-feldspars. It is pink or red to grey color, and coarse grained. It is composed of K-feldspar, plagioclase, quartz, muscovite and biotite.

It is characterized by elliptical to subrounded shape. This granite appears to deflect the syncline in the north of Adi-Bladie and Gua Gubo villages as shown in (Fig. 8).

It cuts the NNE-SSW trending anticline and synclines within the felsic metavolcanic and phyllitic-graphitic schist (Fig. 8). This might indicate emplacement of zelazil granite was related to a major structural feature.

Zelazil granite is traversed by aplitic and pegmatite dikes. A compositional variation from south west to north east was noted during the field observation; it represents variation in the abundance of pinkish k-feldspar and biotite.

3.2.5.6 Aplitic and doleritic dike

The aplitic dikes have wide spread distribution within the felsic metavolcanic, phyllitic – graphitic schist, sericite quartz feldspar schist and granites in the study area. They are light to light gray and light pink colored, fine grained characterized by fractures.

They are massive, forming small linear ridges in places and grade black through shades of grey to pink may corresponding with a transition from mafic to felsic.

The dikes mostly are vertical, sub vertical to horizontal. The aplitic dikes are wide spread in the Hitsas granitic intrusive body abundantly in contrast to the other granitic intrusives in the study area. The thickness varies from 30 to 50 m.

The mafic body is represented by dolerite and felsic rhyolitic dike in the study area shows discordant nature were observed at Kisad Gaba area. The discordant relationship between the rhyolitic and doleritic dike might show mutual intrusive relationships which is indicative of synchronous emplacement of felsic magma and mafic magma.

A prominent N70°E–S70°W trending 2–5m thick dolerite dike has been delineated in the Kisad Gaba intrusive body traced for more than 4km length. The mafic body is medium to fine grained and greenish black to dark black coloured, which show massive nature on exposures.

3.2.5.7 Quartz veins

The quartz veins have wide distribution throughout the study area, especially within the sericite-quartz feldspar schist, felsic-mafic metavolcanics, and granites. It occurs as mall vein ridges, thin and stringers. It is white to milky colored, slightly fractured and discordant to the host rock having NE-SW strike orientation. Most of the veins are highly brecciated and fragments of quartz cover wide area as quartz float. Black tourmaline was noted in association with quartz veins. These occur as thin veins and contain sulphide minerals, light shining muscovite at places and dark stained elongated crystals of tourmaline.

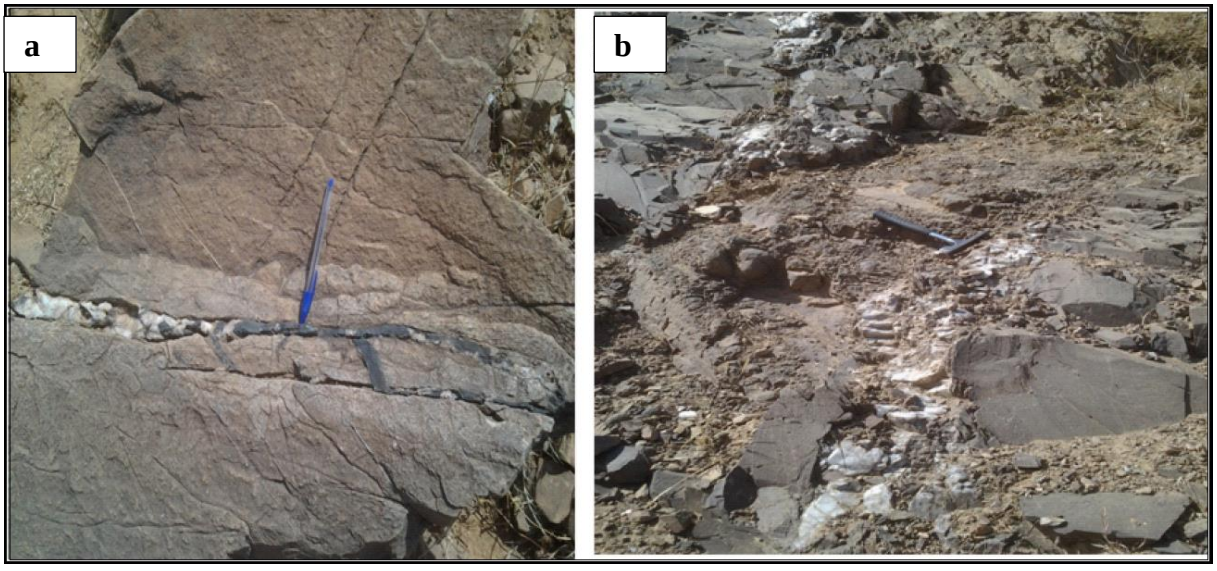

Fig. 13: Field characteristics and occurrence of dolerite, tourmaline and quartz at Kisad Gaba (a) Black tourmaline with quartz vein in metavolcanic rock, (b) Quartz vein cutting dolerite dike west of Kisad Gaba.

3.2.5.8 Pegmatite viens

The pegmatite veins have widespread distribution in Hitsas-Gurungur-Kisad Gaba-Zelazil and Adi-Tsehayo area. These are observed intruding the grey granite and pink granites, comparatively more pronounced in the pink granites at north. They are abundantly exposed in all granite bodies in the area. Thickness of the pegmatite veins vary from 50cm to nearly 10m. In the Kisad Gaba area, they form a conjugate system and invade pervasively the whole

granitic body (Fig. 14b). They occur as veins in the fine to medium grained, massive and coarse grained granites of the study area. The pegmatite veins are pink colored, coarse grained.

Fig. 14: Field characteristics and occurrence of pegmatite at Kisad Gaba (a) folded pegmatite cutting the pink granite (b) and (d) Conjugate Pegmatite vein in Kisad Gaba (coarse grained) pervasively invade the granite body, (c) concordant pegmatite vein cutting weathered granite

3.2.6 Sedimentary rocks

The sedimentary rocks are part of the Mesozoic-Palozoic sedimentary deposited above the metamorphic terranes. These are mainly composed of conglomerate, reddish sandstone, siltstone, chert, and thin lateritic iron at the top. They occurred as flat plateau with hills, ridges and at places as remnant outcrops capping the granites.

3.2.7 Geological Structures in the study area

Thrust and prominent linear features are the major structural elements depicted in the regional geological map of the area. The lithostratigraphy of the rocks generally strikes in the northeast direction except local variations due to structural disturbance and granitic intrusives. The eastern contact of the mafic ultramafic rock in the north western part of the study area is marked by tectonic thrust fault and steep shear zones. The thrust fault on the south eastern margin has a NW vergence suggesting tectonic transport. The metavolcano-sedimentary succession in the central part of the study defines regional anticline and syncline folds (Fig. 8). The fold has an axial plain of NE-SW and gently plunges to the NE.

All the lithologies in the study area are transected by several sets of regional lineaments. The lineaments have a trend of NE, NS, NW and EW.

3.2.8 Mineralization

The main mineralization in the study area includes placer gold, volcanogenic massive sulphides. Placer gold, pyrite and tourmaline bearing-quartz veins were observed in the surface exposures during the field work. Small outcrop of tourmaline veinlet hosted in quartz veins is exposed in the southwest and southern part of the study area.

3.2.8.1 Placer Gold

Intensive small scale artisanal placer gold mining is exercised by the local people in the study area and surroundings. Alluvial stream sediment is extensively panned by the artisanal miners to extract gold. Besides, gold is recovered by crushing quartz veins from surface and tunnels, and hand picking during the rainy season. Gold panning is a means of subsistence for many thousands of the local people. Elluvial diggings on a gentle hill, with no bedrock workings apparent and several areas of extensive elluvial active artisanal gold workings are present in the Hitsas, Gurungur, and Kisad Gaba areas part including bedrock workings at places. All the drainage systems in the area are engaged by extensive gold panning activity and there are some potential alluvial placer gold deposit indications along the banks of major rivers. The current exploration activities around the study area has revealed a shear zone –hosted, structurally controlled auriferous quartz veins of gold.

Fig. 15: Artisinal workings and gold panning at Hitsas and Kisad Gaba

(b) and (d) showing extensive shallow artisanal workings on low lying flat topography, (a), (c) and (f) gold panning along the river banks, **(e)** Panned gold nuggets hosted in graphitic schist

3.2. 8.2 Sulfide mineralization

The dominant sulfide minerals observed are pyrite, malachite and chalcopyrite. They occur on the surface exposures and wall rocks and as veinlets within the quartz veins. Pyrite is common in surface rocks along with quartz vein and dolerite dike at Kisad Gaba.

Currently, exploration activities by mining organizations revealed occurrence of volcanogenic massive sulphide mineralization in Adi-Bladie area, massive gossan in Barnabas, and an old malachite excavation in Hitsas area (Harvest, 2010).

The gossan outcrops are enveloped in very low density, rusty weathered limonitic siliceous outcrops that appear to be siliceous tuffs or sediments. It has an average thickness of 3 meters and contains significant amounts of gold. The gossan is represented by variegated colours of dominantly black, reddish brown and yellow and forms flat topography (Fig. 16).

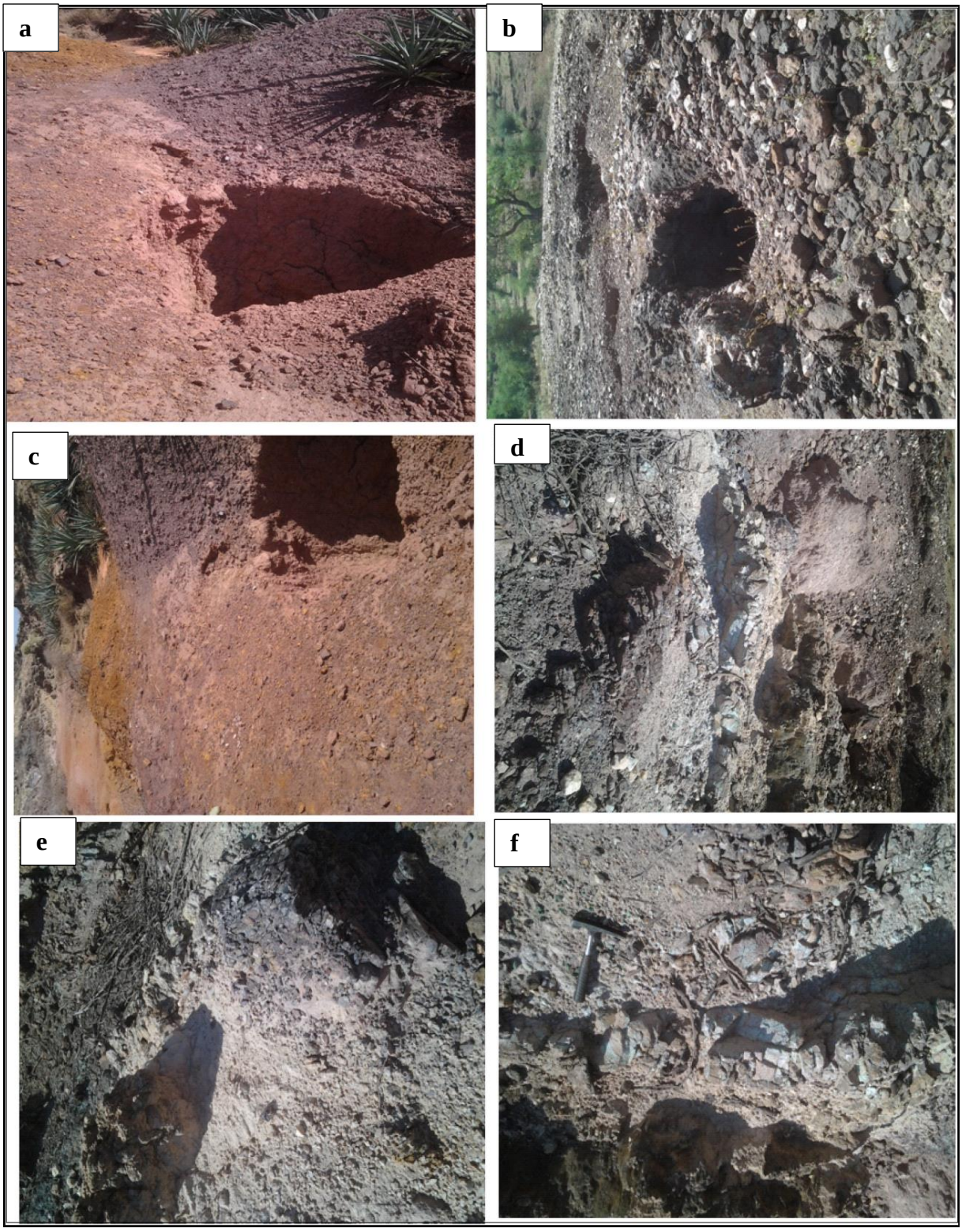

Fig. 16: field characteristics of gossan, workings for gold panning and mineralization at Kisad Gaba

(a), (b), and (c) gossan occurrences and hand dug well for gold panning at Kisad Gaba area; (d) and (f) malachite, (e) Kaolinite alteration (white color)

4. PETROGRAPHY

The granites of the study area are represented dominantly by grey and pink granites as discussed earlier in the previous chapter and the main emphasis is given on them.

The most common mineral assemblage is plagioclase (20–30%), K-feldspar (30-40%), quartz (20–30%), biotite (<5%), with minor hornblende (<2%) and muscovite (<1%). Accessory minerals include; zircon, allanite, apatite, rutile, titanite, pyrite, and opaque phases of Fe-Ti oxides (magnetite and ilmenite). The alteration features are quite common and represented by chloritization of biotite and sericitization of plagioclase and K-feldspar were apparent.

The quartz crystals have undulatory extinction which may suggest that it is affected by deformation. The quartz occurs as rounded to sub-hedral crystals. Quartz appears as clusters between the feldspars and granophyric intergrowth of quartz and feldspar were also observed.

The plagioclase is mostly subhedral-euhedral and zoned with laths. The euhedral to subhedral phenocrysts of plagioclase are common, and zoning and twinning are typical. The zoned plagioclase with laths indicates that a magmatic origin with alteration of sericite showing a mesh texture. Some of the plagioclase grains contain inclusions of subrounded quartz and biotite. The dark high relief radiating nature and euhedral within the biotite is zircon as pleochroic haloes. The presence of hydrous mineral muscovite, chlorite and biotite may indicate a retrograde metamorphism phase caused by fluids.

K-feldspars are dominated by microcline, orthoclase, and microcline-perthite and occur as subhedral to anhedral grains. In the perthite, the exsolved plagioclase component occurs within the host microcline as microscopic lamellae.

The presence of microcline and perthite indicate unmixing of sodium and potassium feldspars. The swelling of albite within microcline (orthoclase) may indicate stages of granite magmatism. The micro perthitic to perthitic intergrowth were also observed in the twin lamellae of K-feldspar and plagioclase may be due to deformation.

Biotite display oxide replacement around the rims and have a pleochroic haloes of radioactive element (zircon). The alteration of biotite to chlorite was a well observed phenomenon that occurs at the outer periphery. Accessory minerals include; zircon, allanite, apatite, rutile, titanite, and common Fe-Ti oxides.

Titanite has a typical double wedge or diamond shape and is typically light brown, and has very high relief. Zircon is enclosed within the biotite as euhedral to sub hedral and with

apatite crystals around it. Zircon has relief considerably higher than the titanite. The uranium and thorium content of zircon causes development of pleochroic radiation halos around it. Allanite show a concentric zoning mostly resulted from changing mineral composition during successive stages of growth. Allanite may contain large amounts of Th and U, which could sustain considerable radiation damage.

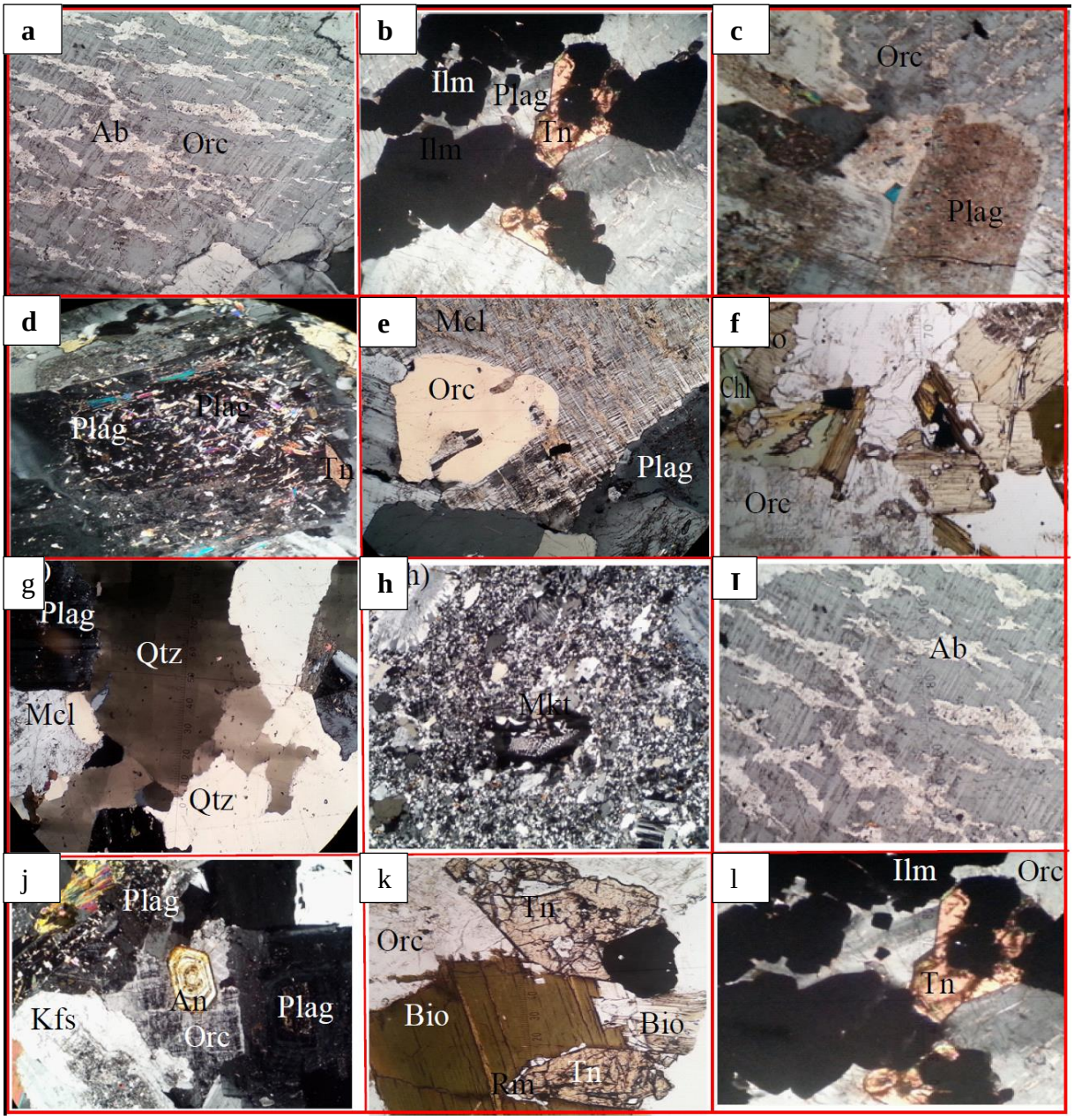

Fig. 17: Petrographic characteristics of the studied granites and metavolcanic

(a, i) albite swelling within K-feldspars (Kisad Gaba)

(c, d) mesh textured zoned plagioclase and altered to sericite (from Hitsas)

(f, k) zircon enclosed within biotite (from Kisad Gaba)

(b, k, l) diamond shape titanite (Hitsas)

(i, j) microperthitic to perthitic intergrowth in K-feldspar (from Gurungur)

(g) Undulatory extinction in quartz affected by deformation

(j) zoned allanite with cracks (from Hitsas)

5. ANALYTICAL METHODS

5.1. U–Pb analytical procedures

Following the map compilation at a scale of 1:10,000, one metavolcanic and seven granite rock samples (1 to 4kg) were collected to represent the main granites and metavolcanic rocks. Three representative granite samples (ET-13-3, ET-13-4 and ET-13-7) from Hitsas, Gurungur and Kisad Gaba areas were selected for U-Pb dating.

A total analysis of 37 grains of zircon and 13 titanite grains were selected for U-Pb dating analysis from these three localities within the study area. Zircon and titanite were chosen as the most suitable minerals to estimate the crystallization age of granites (Corfu, 2004).

Samples for isotope dilution – thermal ionization mass spectrometry (ID-TIMS) were processed at the Department of Geosciences, University of Oslo, Norway, using standard separation techniques. The standard techniques include crushing to a grain size of less than 250 μm using a jaw crusher and a percussion mill. The zircons and titanite were separated from the <250μm fraction by a combination of Wilfley-table washing, heavy liquid separation (diiodomethane), magnetic-separation with a Frantz isodynamic separator (magnetic and non-magnetic were separated in two different cups). The non-magnetic zircon and titanite fraction with the size of <250μm was then purified by hand picking under a binocular microscope.

The non-magnetic fraction at 1.5 to 1.8 A were considered for age dating and then selected multigrain zircon grains were dissolved in bomb Teflon capsul. All were abraded before analysis (Krogh, 1982) and details are elaborated in (Corfu, 2004).

After abrasion the grains were washed in an ultrasonic bath. Zircons were weighted and loaded and spiked with a ^{205}Pb–^{235}U mixture. After that it was placed into a bomb, dissolution for five (5) days at 190^0c. The chemical separation of Pb and U on columns (ion-exchange resin) followed the method of (Krogh, 1973). The Pb and U were measured with a single Re filament with H_3PO_4 and silica gel. The U and Pb isotope ratios were obtained using a Finnigan MAT 262 multicollector mass spectrometer. The isotopic ratios were corrected for mass fractionation, blank and initial lead, using the (Stacey and Kramer, 1975) model Pb composition. The data reduction, age calculation was done using ISOPLOT (Ludwig 2003); age uncertainties in relation to the concordia intercept are at 2σ.

The Concordia age routine of Ludwig (Isoplot) calculates the most-probable age for a data-point (or weighted-mean data-point) on a concordia diagram, and the age uncertainties in

relation to the Concordia are at 2σ. The results of U-Pb zircon and titanite dating age are listed in Table 1 and illustrated in Fig. 18a-e; error for weighted mean ages of samples is quoted at 95% confidence.

5.2 Whole-rock geochemical analyses

Eight samples were selected to carry out geochemical analysis. Major and minor element oxides, Trace elements and REEs were carried out by fusion inductively coupled plasma (FUS-ICP) and fusion mass spectrometry (FUS-MS) at ACTLABS (Ancaster, Ontario, Canada), (8 samples). More information on the procedure, precision and accuracy of ACTLABS FUS- ICP and FUS-MS analyses could be found at www.actlabs.com.

The mass balance is employed as an additional quality control technique and elemental totals of the oxides were between 98 to 100.8%. All new geochemical datas of major, minor trace and rare earth elements compositions are provided in Table 2,3,4 and geochemical classification of the granites with different classification methods illustrated in (Fig. 19-28). The tectonic discrimination diagrams for the classification of the granites setting are also shown in (Fig. 28) using the GCDKit 3.00 version software.

The major, minor oxides with detection limits and trace elements and REE detection limits could be found at www.actlabs.com.

6. RESULTS

6.1 U-Pb data and zircon-titanite characteristics

The granitic samples selected for dating were from Hitsas (ET-13-3), Gurungur (ET-13-4) and Kisad Gaba (ET-13-7). The results and zircon and titanite characteristics are discussed below in detail:

6.1.1 Hitsas granite (Sample ET-13-3)

This sample was taken from the southwestern of the studied area (Hitsas). It is fine to medium grained, slightly porphyritic and characterized with dark colored enclaves. The selected zircons are euhedral, sub-prismatic with tips, long tips having length/width ratios 2:1 and 3:1, colorless, transparent. 14 zircon and 9 titanite grains were selected for dating analyses. The zircon grains also contain black inclusions that occur at the corner of the zircon grains, however; some of the zircon grains are light red under the binocular microscope. The titanite grains were dark brown to light yellowish in color. The titanite grains are subhedral to anhedral in shape.

Majority of the studied granites contain zircon grains and titanite grains which we have chosen as the most suitable minerals to estimate the crystallization age of the granites.

These zircon crystals contain a uranium concentration of 23 - 271ppm, the highest U concentration is from zircon grains of 384/1 and lowest concentration 23ppm from titanite grains of 384/S63. The Pb concentration 7-28ppm and Th/U ratios are relatively very high varies from 0.37 - 4.06 (average 2.215).

All fourteen (14) zircon grains have similar $^{206}Pb/^{238}U$ ages (621.7-624.2 Ma), $^{207}Pb/^{235}U$ ages (622.9-624.9Ma) and $^{207}Pb/^{206}Pb$ ages (627.1-628.9 Ma). The nine (4) titanite grains have also similar ages of $^{206}Pb/^{238}U$ ages (622.3-626.1), $^{207}Pb/^{235}U$ ages (619.9-624.1) and $^{207}Pb/^{206}Pb$ ages (611.2-613.7) respectively.

Two fractions of zircon analysis record slightly younger 206Pb/238U age of 623.8±1.3 Ma (fraction 384/3) and 621.7±1.2 Ma (fraction 384/2). The former has high common 206 Pb proportion of 1.5 and a lower proportion of $^{206}Pb/^{204}Pb$ ratio while the later has low common 206Pb and higher proportion of $^{206}Pb/^{204}Pb$ ratio (table 1), this may indicate effect of later coming alterations.

The three titanite fractions of 384/S62 brown color, mechanically abraded yielded $^{206}Pb/^{238}U$ age of 625.2 Ma, yellow to brown two fractions of 384/S63 yield age of 626.1Ma, and brown

color four fractions of 384/S65 yield an age of 622.3 Ma. Therefore, Titanite has a closure temperature below that of zircon for the U–Pb isotope system; hence this provides the minimum crystallization age estimate which is very close to the zircon age.

The 14 zircon grains and 9 titanite grains analysed form one coherent 3 points and tightly cluster on concordia diagram (Fig. 18a) yielding a concordia mean age of 624.07 ± 0.72 Ma (95% conf. MSWD = 0.1). All the 4 points anchored at 0 ± 0 Ma yield mean age of 627.5 ± 1.1 Ma, with mean standard weighted deviation of 0.36 and data-point error ellipses of 2σ. In the concordia diagram (Fig. 18a); all of the analyses are normally concordant with the concordia curve with the discordance of less than 2%.

The four abraded fractions of zircon define a Concordia with MSWD 0.36 intersecting at 627.5±1.1 Ma and are interpreted as the crystallization age of the Hitsas granite. The three titanite(3) and four(4) zircon fractions anchored at 0 ± 0 Ma gave concordant age of 627.5 ± 1.1 Ma with MSWD = 0.27 (Fig. 18b). These two ages are consistent with each other and they are interpreted as the crystallization age of the Hitsas granite.

6.1.2 Gurungur granite (Sample ET-13-4)

This sample was collected from 2km north east of Hitsas and eight zircon grain measurements were selected for dating (Table 1) and presented on a concordia diagram plot (Fig 18c). They are colorless, stubby, and transparent, and the analyzed grains for dating were labeled as 384/5,384/6,384/7 and 384/8. The zircon grains show black inclusions, easily breakable during picking due to high content of uranium and show euhedral shape with long tips. Some of the grains show also a marginal pitting and fractured with length to width ratio of 3:1.

The uranium concentration ranges from 473- 1424 ppm. The Th/U ratios are relatively low from 0.26 to 0.35 (on average 0.305) compared to Hitsas. Eight (8) zircon grains have similar $^{206}Pb/^{238}U$ ages (622.4- 624.2Ma), $^{207}Pb/^{235}U$ ages (623.6-624.6 Ma) and $^{207}Pb/^{206}Pb$ages (625.9-631.7 Ma).

The four points concordant analysis form tightly clustered on the concordia diagram and yield a weighted mean $^{206}Pb/^{238}U$ age of 624.24±0.60Ma (95% confidence, MSWD=0.62), (Fig. 18c)but it is discordant. This is interpreted as the crystallization age of Gurungur granite.

6.1.3 Kisad Gaba granite (Sample ET-13-7)

This sample was collected from the northern part of Kisad Gaba and it is coarse grained porphyritic granite. 18 zircon and 4 titanite grains were selected for analyses and the recorded age is presented on the concordia diagram (Fig. 18d, e).

The analyzed samples for dating were labeled as 384/5,384/6,384/7 and 384/8 and zircon and titanite grains were chemically abraded and air abraded in which the results are presented in table 1. The zircon grains are fractured easily breakable due to the presence of high uranium concentration. They are very transparent, light yellow-blue color, euhedral, long tip prismatic shape with length to width ratio 4:1and with black inclusions.

These display a variation in Uranium concentrations ranging from 80-377ppm, Th/U ratios are relatively very high (0.66 to 5.67) and has the highest Thorium-Uranium ratios compared to others. The highest Thorium-Uranium ratio is 5.67 from titanite grains whereas the lowest concentration is from zircon grains.

The 18 zircon grains have similar ages of $^{206}Pb/^{238}U$ (604.2 - 608.6 Ma), $^{207}Pb/^{235}U$ (605-609.2 Ma) and $^{207}Pb/^{206}Pb$ (609.8-611.9 Ma). The four titanite grains yielded a $^{206}Pb/^{238}U$ (611.8- 609.8), $^{207}Pb/^{235}U$ (610.9-609) and $^{207}Pb/^{206}Pb$ (606.2-607.7) ages respectively.

The 2 titanite and 4 zircon grains anchored at 0 ± 0 form a statistically precise age determination. The weighted mean 206Pb/238U age is 610.7 ± 1.1 Ma with a MSWD 0.44 (Fig. 18d).

The four point's concordant analyses form tight cluster on the concordia diagram and yield a weighted Mean $^{206}Pb/^{238}U$ age 606.1 ± 2.6 Ma 95% conf. MSWD = 6.2 (Fig. 19e). Hence, they define a $^{206}Pb/^{238}U$ age of 606.1 ± 2.6 Ma and can be considered as the time of crystallization of the kisad Gaba granite. Thus, the two concordant data points constrain the crystallization age of kisad Gaba granite at 606.1 ± 2.6 Ma and 610.7 ± 1.1 Ma respectively. The Kisad Gaba granite is the youngest of the other two granites.

Table 1: The ID-TIMS U- Pb data of zircon and titanite grains from the studied granites

Sample Code	Fraction Analysed	Properties	Wt [mg]	Pbt [ppm]	U [ppm]	Th/U	Pbc [ppm]	Pbcom [pg]	206/204	207/235	±2σ [abs]	206/238	±2σ [abs]
Granite from Hitsas													
ET-13-3	384/1	Z sp ca 1gr	9	28	271	0.37	0.00	1.3	11691	0.85039	0.00229	0.10168	0.00022
ET-13-3	384/2	Z ltp 1gr	11	22	218	0.39	0.00	1.0	15330	0.84677	0.00212	0.10124	0.00021
ET-13-3	384/3	Z tp 3gr	15	18	172	0.40	0.00	1.5	11166	0.85042	0.00233	0.10160	0.00022
ET-13-3	384/4	Z eh sp 9gr	65	25	244	0.39	0.15	11.9	8486	0.85038	0.00208	0.10167	0.00021
ET-13-3	384/S62	Ti br a 3gr	68	7	29	3.64	1.71	119.5	123	0.84646	0.02207	0.10184	0.00041
ET-13-3	384/S63	Ti ybr 2gr	32	7	23	3.72	2.15	71.5	83	0.84897	0.03480	0.10200	0.00057
ET-13-3	384/S65	Ti a br 4gr	77	8	30	4.06	2.01	157.7	109	0.84140	0.02590	0.10135	0.00044
Granite from Gurungur													
ET-13-4	384/5	Z ltp 1gr	5	55	534	0.35	0.00	1.2	13800	0.84987	0.00214	0.10167	0.00021
ET-13-4	384/6	Z lp 1gr	1	142	1424	0.26	0.00	0.8	11395	0.84969	0.00241	0.10138	0.00023
ET-13-4	384/7	Z lp 2gr	4	65	638	0.33	0.00	1.1	14520	0.84957	0.00229	0.10144	0.00022
ET-13-4	384/8	Z bp 4gr	6	48	473	0.29	0.00	1.5	12028	0.84805	0.00210	0.10136	0.00021
Granite from Kisad Gaba													
ET-13-7	384/9	Z ca spr 1gr	7	41	377	0.66	0.13	2.9	5634	0.81599	0.00200	0.09826	0.00019
ET-13-7	384/10	Z ca sp 3gr	14	32	293	0.68	0.00	1.9	13230	0.81911	0.00198	0.09868	0.00020
ET-13-7	384/11	Z ca sp 4gr	6	41	374	0.69	0.10	2.6	5339	0.82206	0.00560	0.09901	0.00055
ET-13-7	384/12	Z ca pi 10gr	17	29	270	0.67	0.03	2.6	11106	0.81955	0.00195	0.09878	0.00020
ET-13-7	384/S67	Ti a br 1gr	7	22	90	4.27	3.49	26.6	166	0.82517	0.01477	0.09956	0.00031
ET-13-7	384/S69	Ti a br 3gr	10	22	80	5.67	2.04	22.6	238	0.82175	0.01034	0.09921	0.00026

Table 1: Continued……..

Sample Code	Fraction Analysed	Properties	Wt [mg]	rho	207/206	±2σ [abs]	206/238	±2σ [abs]	207/235	±2σ [abs]	207/206	±2σ [abs]	Disc.
Granite from Hitsas													
ET-13-3	384/1	Z sp ca 1gr	9	0.88	0.06066	0.00008	624.2	1.3	624.9	1.3	627.1	2.7	0.5
ET-13-3	384/2	Z ltp 1gr	11	0.91	0.06066	0.00006	621.7	1.2	622.9	1.2	627.2	2.3	0.9
ET-13-3	384/3	Z tp 3gr	15	0.87	0.06071	0.00008	623.8	1.3	624.9	1.3	628.9	2.9	0.9
ET-13-3	384/4	Z eh sp 9gr	65	0.95	0.06066	0.00005	624.2	1.3	624.9	1.1	627.3	1.7	0.5
ET-13-3	384/S62	Ti br a 3gr	68	0.11	0.06028	0.00156	625.2	2.4	622.7	12.1	613.7	55.0	-2.0
ET-13-3	384/S63	Ti ybr 2gr	32	0.07	0.06037	0.00248	626.1	3.4	624.1	19.0	616.8	86.1	-1.6
ET-13-3	384/S65	Ti a br 4gr	77	0.11	0.06021	0.00184	622.3	2.7	619.9	14.2	611.2	64.8	-1.9
Granite from Gurungur													
ET-13-4	384/5	Z ltp 1gr	5	0.92	0.06062	0.00006	624.2	1.2	624.6	1.2	625.9	2.2	0.3
ET-13-4	384/6	Z lp 1gr	1	0.86	0.06079	0.00009	622.5	1.3	624.5	1.3	631.7	3.1	1.5
ET-13-4	384/7	Z lp 2gr	4	0.89	0.06074	0.00008	622.8	1.3	624.4	1.3	630.1	2.7	1.2
ET-13-4	384/8	Z p 4gr	6	0.92	0.06068	0.00006	622.4	1.2	623.6	1.2	627.9	2.1	0.9
Granite from Kisad Gaba													
ET-13-7	384/9	Z ca spr 1gr	7	0.90	0.06023	0.00007	604.2	1.1	605.8	1.1	611.9	2.4	1.3
ET-13-7	384/10	Z ca sp 3gr	14	0.93	0.06020	0.00006	606.7	1.2	607.6	1.1	610.9	2.0	0.7
ET-13-7	384/11	Z ca sp 4gr	6	0.85	0.06022	0.00021	608.6	3.2	609.2	3.1	611.3	7.7	0.5
ET-13-7	384/12	Z ca p 10gr	17	0.94	0.06017	0.00005	607.3	1.2	607.8	1.1	609.8	1.8	0.4
ET-13-7	384/S67	Ti a br 1gr	7	0.16	0.06011	0.00106	611.8	1.8	610.9	8.2	607.7	37.7	-0.7
ET-13-7	384/S69	Ti a br 3gr	10	0.24	0.06007	0.00074	609.8	1.5	609.0	5.8	606.2	26.2	-0.6

Z= zircon; Ti= titanite; ltp= long tip prismatic; P= prismatic; sp= short prismatic; lp= long prismatic; eh= euhedral; a= abraded; ca= chemically annealed; br= brown; ybr= yellow brown; gr= grain; Pbc= total common Pb in sample (initial +blank); rho= corrected for fractionation; D=discordancy; wt= weight

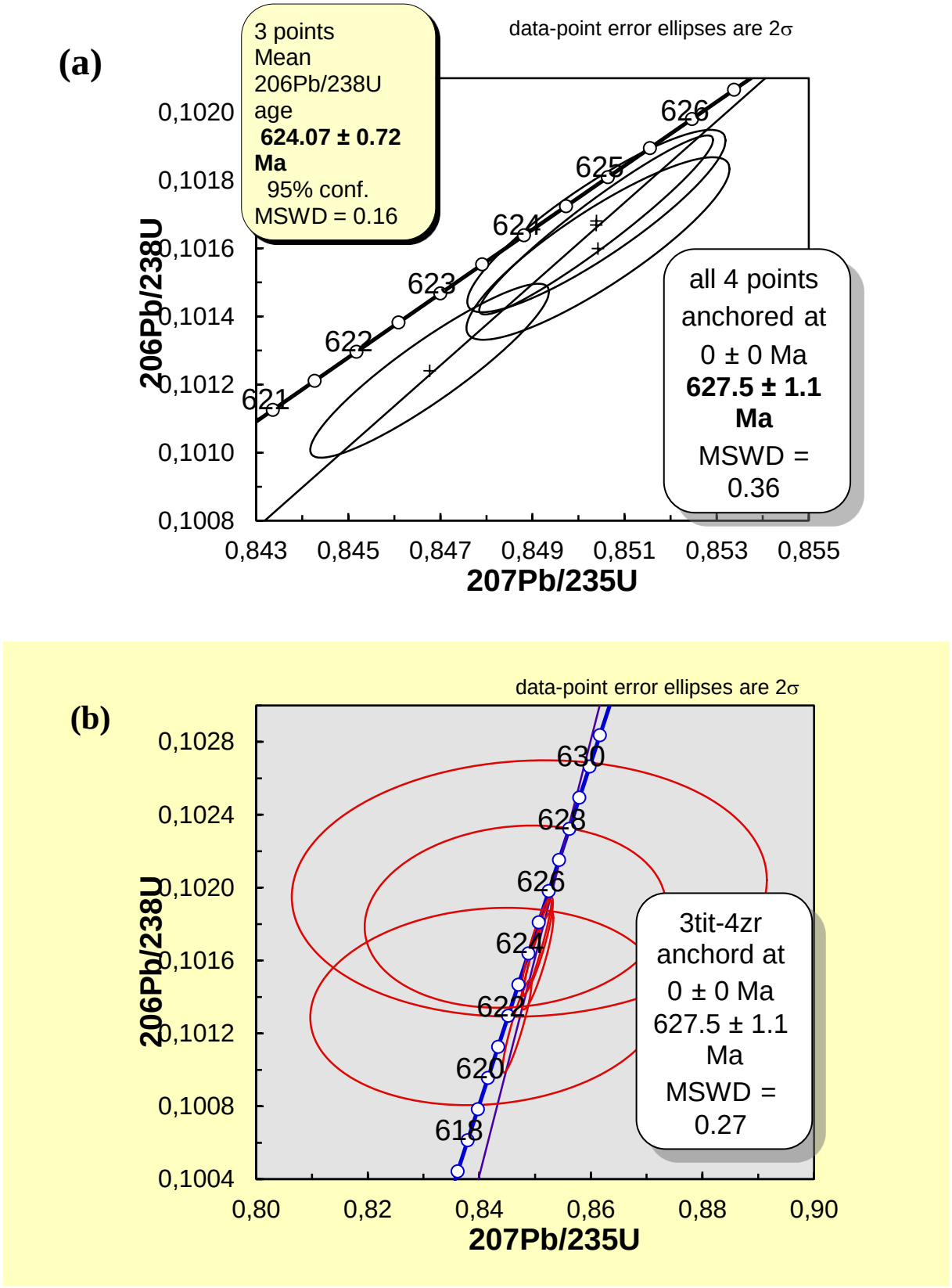

Fig. 18a, b 206Pb/238U vs207Pb/235U Concordia diagrams with multi grain analysis of zircon and titanite fraction from Hitsas granites (sample ET-13-3).

(c)

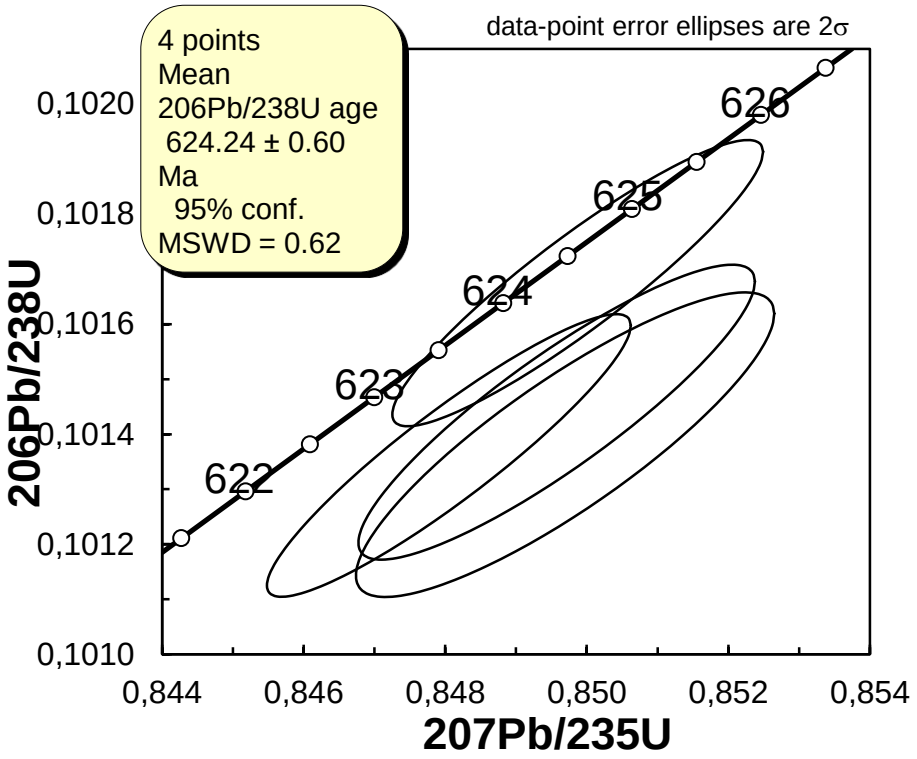

Fig. 18c 206Pb/238U vs207Pb/235U concordia diagrams with grain analysis of zircon from Gurungur granite (sample ET-13-4).

(d)

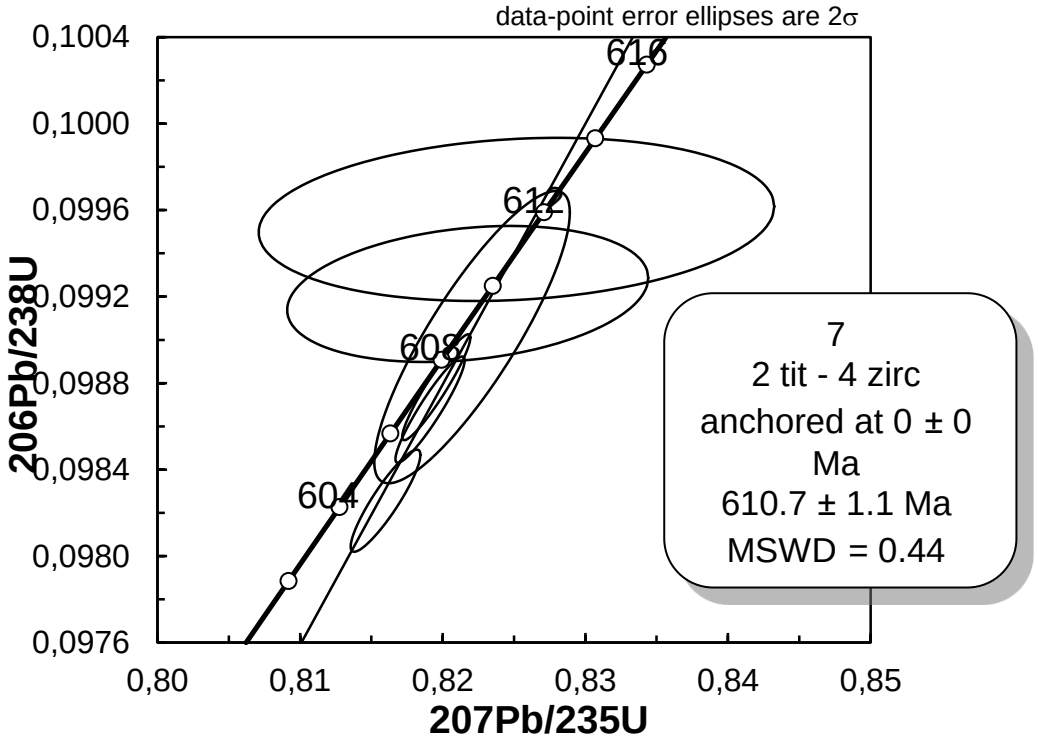

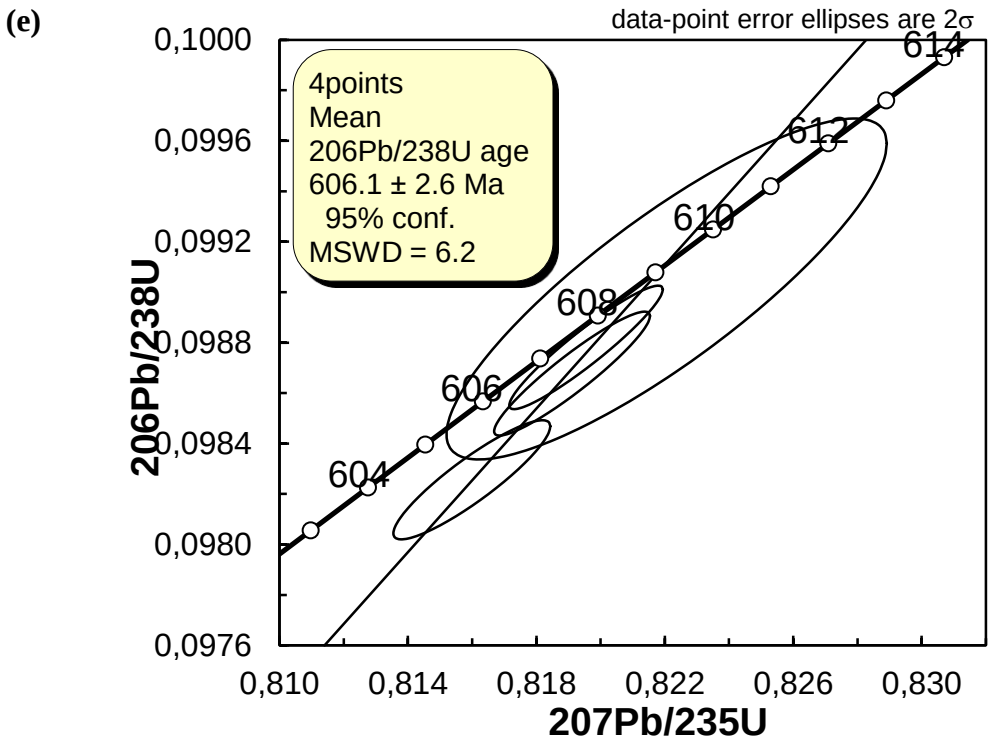

Fig. 18d U-Pb concordia diagrams for 4zircon grains and 2 titanite analyses, (e) zircon U-Pb concordia diagrams 4points from Kisad Gaba granite(sample ET-13-7) respectively.

6.2 Geochemistry

The geochemical characteristics of one metavolcanic sample and the Hitsas granite, Gurungur granite, and Kisad Gaba granites was done to characterize their chemical composition, geochemical classification, chemical affinity, and tectonic setting. The major oxides and selected trace and rare earth elements are given in table 2, 3 and 4 respectively.

6.2.1 Major element geochemistry

Major element oxides selected were plotted against SiO_2 concentrations in Harker variation diagrams (Fig. 19). Most of the samples are characterized by moderate to high silica contents (67.21 to 75.51wt. %) and high contents of Al_2O_3 (12.35 - 15.83 wt. %). The granites from Hitsas, Gurungur, Kisad Gaba and one metavolcanic from Kisad Gaba show higher SiO_2, K_2O and Na_2O, but lower TiO_2, Fe_2O_3, MgO, Al_2O_3, CaO and P_2O_5 (Table 2; Fig. 20). Overall, the studied samples show a general trend of decreasing Al_2O_3,TiO2, Fe_2O_3, MgO, CaO and P_2O_5 with increasing SiO_2 (Fig. 20). The K_2O and Na_2O contents show an increase even if there are

scattered and irregular distribution patterns. On Harker variation diagrams Al_2O_3, Fe_2O_3, CaO, P_2O_5 and MgO show good correlation with SiO_2 content. The TiO_2 shows a scattered negative correlation with SiO_2 content. The Na_2O shows small data spread and poor correlation in contrast to K_2O, whereas K_2O show a wider data scatter and positive correlation. These linear trends probably indicate that the elements are not significantly changed from their primary abundances or indicating normal igneous trends. The irregular trends may also indicate a magma contamination during asthenospheric uprise.

The three grey granite samples from Hitsas (Sample ET-13-1;ET-13-2 and ET-13-3) show wide variation in silica contents (SiO_2 67.1 to 75.17 %; average 70.97 %) and are poor in Fe_2O_3(T) (0.94 to 2.23 %; av. 1.73%), CaO (0.7 to 2.87%; av. 1.81%), MgO (0.08 to 1.67%; av. 0.86) and MnO (0.046 to 0.058%; av. 0.053%), TiO_2 (0.082 to 0.331%; av. 0.21%) and P_2O_5 (0.02 to 0.15%; av.0.093%).

The three samples from Kisad gaba granites show relatively narrow variation in SiO_2 content (70.87 to 73.16%; av. 72.34%), having almost the same high contents of Al_2O_3 (13.37 to 15.22 %; av. 14.04 %), Fe_2O_3 (1.73 to 2.02%; av. 1.86%), MgO (0.21 to 0.69 %; av.0.45%), CaO (1.15 to 1.88 %; av. 1.48%), MnO (0.037 to 0.045%; av. 0.041%), TiO_2 (0.32 to 0.335%; av. 0.33%) and P_2O_5 (0.08 to 0.13%; av.0.097%; Table 2).

The Gurungur granite (Sample ET-13-4) show higher SiO_2 content within the same range with other samples. A metavolcanic sample from Kisad Gaba display higher SiO_2 content than the Granite samples, indicating it is more silicic in character. The samples are peraluminous with (A/CNK = 1.36– 1.46 in the granites and 2.77 in the metavolcanic; A/NK= 1.56-1.92 in the granites and 2.85 in the metavolcanic; see Table 2)

6.2.2 Trace element geochemistry

Trace elements concentrations of the studied granites and one metavolcanic rock are listed in Table 3. The selected elements are plotted against SiO_2 (Fig. 20). The Rb, Y and Zr contents increase with increasing of SiO_2, whereas Sr and Ba decrease with increasing of SiO_2. Most of the samples from Hitsas, Gurungur and Kisad Gaba are characterized by enrichment of large lithophile elements (K, Pb and Ba). All the seven granite samples and one metavolcanic sample from the studied area show a very high nickel and chromium concentrations.

The three granite samples from Hitsas granite are characterized by low concentration of Rb (50 to 111 ppm; av. 84.33 ppm), high concentration of Sr (218 to 1564 ppm; av. 913), and high Ba (764 to 1549 ppm; av. 1211.67 ppm). Trace elements Cr (430 to 530 ppm; av.

480ppm), high Cr (430 to 530 ppm; av. 480ppm), very high Ni (2020 to 2630 ppm; av.2263.33ppm) Co low (1-7 ppm; av.4.67ppm) and high Zr (81 to 155 ppm; av. 113.33ppm). The Gurungur granite the Rb content is 90 ppm, Sr 317 ppm and Ba 808 ppm and display high content of Ni from 2280 ppm, Cr 480 ppm, very low Co, Zr and Nb.

In Kisad Gaba granite and Ba ranges (from 689 to 1436; av. 955ppm), Sr ranges (from 257 to 929 ppm; av. 486.67ppm) Rb ranges (from 116 to 171 ppm; av.147 ppm). The maximum Ba content 4985 ppm was from the metavolcanic sample.

On a primitive mantle-normalized multi-element variation diagram (Sun and McDonough, 1989; Fig. 21), all samples are characterized by pronounced negative Nb–Ta– Ti anomalies. An exception for the metavolcanic sample (ET-13-5) with pronounced negative Sr anomaly. Over all the studied samples are characterized by enrichment of large ion lithophile elements (Rb, Ba, K and Pb) and high field strength elements (U and Th) but the high field strength element Y was relatively flat, Zr was slightly depleted and Ti strongly depleted.

6.2.3 Rare earth element geochemistry

Rare Earth elements concentrations of the studied samples were given in detail Table 4.

The concentration of La ranges (16.7 -78.3ppm), Ce (33.6 -139 ppm), Tb <1ppm, Gd (2.04-4.21 ppm), Yb (0.43-1.76 ppm), Eu <2 ppm and a very low Ta (<2 ppm).

The concentration of Y (5.8 to 33 ppm) on average 14.9 ppm is lower than the quoted average value of 40ppm for normal granites. The concentration of Zr (81 to 208 ppm) on average 135.3 ppm, Nb (<0.2 to 12.5 ppm), Yb (0.43 to 3.44) on average 1.42 which is very low and Th (2.57 to 20.9 ppm), U (1.46 to 4.22 ppm) average 2.66 ppm, Pb from 18 to 33 ppm (average 23.38), Sm (2.69 to 6.81 ppm) average 4.42 ppm, Nd (14.2 to 45 ppm), Ce (33.6 to 139 ppm), La (16.7 to 78.3 ppm).

The chonderite –normalized Rare Earth Elements (REEs) diagrams (Boynton, 1984), (Fig. 27) show over all steep patterns characterized by negative slope with over all enrichment of LREE relative to flat Heavy Rare Earth Elements (HREEs). The studied granite samples and one metavolcanic exhibit similar Rare-Earth Elements (REE) distribution patterns. The studied samples are enriched in Light Rare- Earth Elements (LREE) relative to Heavy Rare-Earth Elements (HREE). Two granite samples from Kisad Gaba display a slight decrease in HREEs. The metavolcanic sample (ET-13-5) has 10fold enrichment of Heavy Rare Earth Elements than the granite samples.

6.2.4 Geochemical classification and magmatic affinity

The studied area samples show distribution mainly in the granite field in total alkali-silica (SiO2 versus $Na_2O + K_2O$) diagram (Cox et al., 1979), (Fig. 22), whereas in the total alkali-silica diagram (Middle most, 1994) most samples are clustered mainly in granite field, sample ET-13-1from Hitsas straddle close to the boundary between granite field and the alkali feldspar granite (Fig. 23).

The nomenclature and classification of these samples have also been attempted using other parameters such as cationic Q–P diagram (Debon and Lefort, 1983) i.e., Si/3 – (K+Na+2Ca/3) versus K–(Na+Ca) (not shown), which has shown their close affinity with granite–quartzmonzonite–granodiorite series.

On the AFM plot (Irvine and Baragar, 1971), (Fig. 24) to discriminate between tholeiitic and calc-alkaline suites, all samples occupy the calc-alkaline affinity indicating their (Na_2O+K_2O) rich nature. Similar observation has also confirmed in SiO_2-Feot/MgO plot (Miyashiro, 1974) most of the samples occupy the calc-alkaline series field (Fig. not shown) and on SiO_2-K_2O plot (Peccerillo and Taylor, 1976) all the samples plot occupying the high-K calc alkaline series with exception of (sample ET-13-6) from Kisad Gaba lies close to shoshonitic series (Fig. 25).

The Al_2O_3/ (Na_2O+K_2O) versus Al_2O_3/ ($CaO+Na_2O+K_2O$) binary diagram was used to discriminate peraluminous, metaluminous and peralkaline magma series (Shand, 1943), (Fig. 26). This diagram shows that the studied samples are strongly peraluminous. The A/CNK and A/NK ratios for the majority of the samples are greater than 1.4 and 1.60 (Table 2) respectively.

(Pearce et al., 1984) has proposed a tectonic classification of granites based Rb, Y, Nb, Yb and Ta data. On the Rb versus (Y +Nb) trace elements our studied samples mainly plot in the volcanic arc granite (VAG) and marginally syncollissional granite (Syn-COLG) fields (Fig. 28). On the Rb versus Ta+Yb discriminant diagram (Pearce et al. 1984) all samples plotted in the volcanic arc fields and marginally in the syn-collisional granites. Whereas On the Nb versus Y diagram the samples fall in the volcanic arc granite and syn-collisional granite fields.

Table 2-Major element oxides (Wt. %)

Locality	Hitsas			Gurungur	Kisad Gaba			
Rock	Granite	Granite	Granite	Granite	Metavolcanics	Granite	Granite	Granite
SiO_2	75.17	70.53	67.21	72.58	75.51	73.16	73	70.87
TiO_2	0.082	0.228	0.331	0.115	0.297	0.335	0.32	0.335
Al_2O_3	13.69	15.11	15.83	13.74	12.35	13.37	13.54	15.22
Fe_2O_3	0.94	2.03	2.23	1.2	1.81	1.83	1.73	2.02
MnO	0.058	0.054	0.046	0.053	0.02	0.045	0.041	0.037
MgO	0.08	0.82	1.67	0.24	0.9	0.44	0.21	0.69
CaO	0.7	1.86	2.87	0.68	0.13	1.15	1.4	1.88
Na_2O	4.16	4.56	4.95	4.31	0.31	3.4	3.35	4.31
K_2O	4.5	4.41	3.27	4.5	4.01	5.13	5.19	4.47
P_2O_5	0.02	0.11	0.15	0.05	0.05	0.08	0.08	0.13
LOI	0.14	0.59	0.76	0.56	1.93	0.33	1.19	0.82
Sum	99.54	100.3	99.31	98.02	97.31	99.27	100	100.8
CaO/Na_2O	0.16	0.40	0.57	0.16	0.41	0.33	0.41	0.43
Na_2O/K_2O	0.92	1.03	1.51	0.96	0.08	0.66	0.65	0.96
Na_2O+K_2O	8.66	8.97	8.22	8.81	4.32	8.53	8.45	8.78
K_2O/ Na_2O	1.08	0.97	0.66	1.04	12.94	1.51	1.55	1.04
Fe_2O_3/MgO	11.75	2.48	1.34	5.7	2.0	4.2	8.24	2.9
A/NK	1.58	1.68	1.92	1.56	2.85	1.56	1.58	1.73
A/CNK	1.46	1.39	1.42	1.44	2.77	1.38	1.36	1.42

Table 3: Trace Elements (ppm)

Locality	Hitsas			Gurungur	Kisad Gaba			
Rock	Granite	Granite	Granite	Granite	Metavolcanics	Granite	Granite	Granite
Ag	<0.5	1.7	0.8	0.7	0.5	1.4	1.0	0.9
As	< 5	7	< 5	< 5	18	< 5	< 5	< 5
Ba	764	1322	1549	808	4985	689	740	1436
Be	3	4	3	3	3	3	3	4
Bi	<0.1	<0.1	<0.1	<0.1	<0.1	<0.1	<0.1	<0.1
Co	1	6	7	2	1	4	3	4
Cr	430	530	480	480	150	600	620	400
Cu	< 10	40	< 10	< 10	10	10	20	20
Cs	2.3	1.6	0.5	0.5	0.4	1.1	1.0	1.1
Ga	16	18	17	16	12	17	18	18
Ge	1.5	1.5	1.3	0.8	1.0	1.7	1.2	1.2
Hf	2.8	3.4	2.8	2.9	1.9	4.6	4.5	3.4
Mo	< 2	3	< 2	< 2	5	< 2	< 2	< 2
Nb	5.3	<0.2	3.5	1.7	<0.2	12.5	10.1	4.9
Ni	2020	2630	2140	2280	800	2850	3430	1810
In	<0.1	<0.1	<0.1	<0.1	<0.1	<0.1	<0.1	<0.1
Pb	30	33	18	23	18	20	21	24
Rb	111	92	50	90	70	171	154	116
Sb	<0.2	<0.2	<0.2	0.3	<0.2	<0.2	<0.2	<0.2
Sc	2	4	4	2	10	2	3	3
Sn	1	< 1	< 1	< 1	< 1	1	2	< 1
Sr	218	957	1564	317	13	274	257	929
Ta	<0.1	<0.1	<0.1	<0.1	<0.1	<0.1	<0.1	<0.1
Th	7.70	5.61	2.57	9.97	3.62	18.7	20.9	7.99
Tl	0.37	0.35	0.14	0.14	<0.05	0.51	0.37	0.31
U	2.60	1.99	1.69	2.74	1.46	4.22	3.94	2.63
V	6	39	43	15	18	24	33	34
W	<0.5	2.9	<0.5	0.6	2.1	<0.5	0.7	<0.5
Zn	40	80	30	< 30	40	40	30	40
Zr	81	155	104	128	93	179	208	135
Y	10.9	11.1	7.4	13.1	33.0	19.8	18.1	5.8
K/Rb	486.48	565.22	778	606.67	738.57	94.74	407.14	456.03
Rb/Sr	0.51	0.10	0.03	0.28	5.38	0.62	0.60	0.12
Ba/Sr	3.50	1.38	0.99	2.55	383.50	2.51	2.88	1.55
Rb/Ba	0.15	0.07	0.03	0.11	0.01	0.25	0.21	0.08
Ba/Rb	6.88	14.37	30.98	8.98	71.21	4.03	4.81	12.38

Table 4: (REEs) Rare Earth Elements (ppm)

Locality	Hitsas			Gurungur	Kisad Gaba			
Rock	Granite	Granite	Granite	Metavolcanics	Granite	Granite	Granite	Granite
La	16.7	20.6	16.7	29.0	23.4	69.6	78.3	25.7
Ce	34.3	38.2	33.6	51.1	42.9	127	139	47.2
Pr	3.98	4.79	4.24	6.43	5.66	13.5	14.5	5.42
Nd	14.2	19.1	16.8	22.6	23.7	42.5	45.0	19.2
Sm	2.69	3.90	2.81	4.16	5.85	6.13	6.81	3.01
Eu	0.513	0.926	0.742	0.721	1.31	0.852	0.882	0.688
Gd	2.13	2.48	2.04	2.46	4.68	4.21	3.74	1.86
Tb	0.33	0.35	0.28	0.39	0.84	0.62	0.57	0.23
Dy	1.77	1.89	1.35	2.20	5.31	3.25	3.00	1.00
Ho	0.36	0.38	0.25	0.41	1.11	0.62	0.58	0.18
Er	1.02	1.03	0.62	1.17	3.35	1.72	1.66	0.49
Tm	0.153	0.155	0.087	0.168	0.494	0.254	0.243	0.069
Yb	1.10	1.17	0.61	1.16	3.44	1.76	1.69	0.43
Lu	0.175	0.174	0.096	0.161	0.549	0.268	0.260	0.074
CeN/YbN	8.07	8.46	14.24	11.39	3.23	18.67	21.26	28.36
LaN/SmN	3.90	3.32	3.74	4.39	2.52	7.14	7.23	5.37
LaN/YbN	10.24	11.89	23.52	16.86	4.59	26.67	31.22	40.24
GdN/YbN	1.56	1.71	2.69	1.71	1.09	1.92	1.78	3.48
CeN/SmN	3.09	2.36	2.88	2.96	1.77	4.99	4.92	3.78
Eu/Eu*	6.98	12.60	10.09	9.81	17.82	11.59	12	9.36

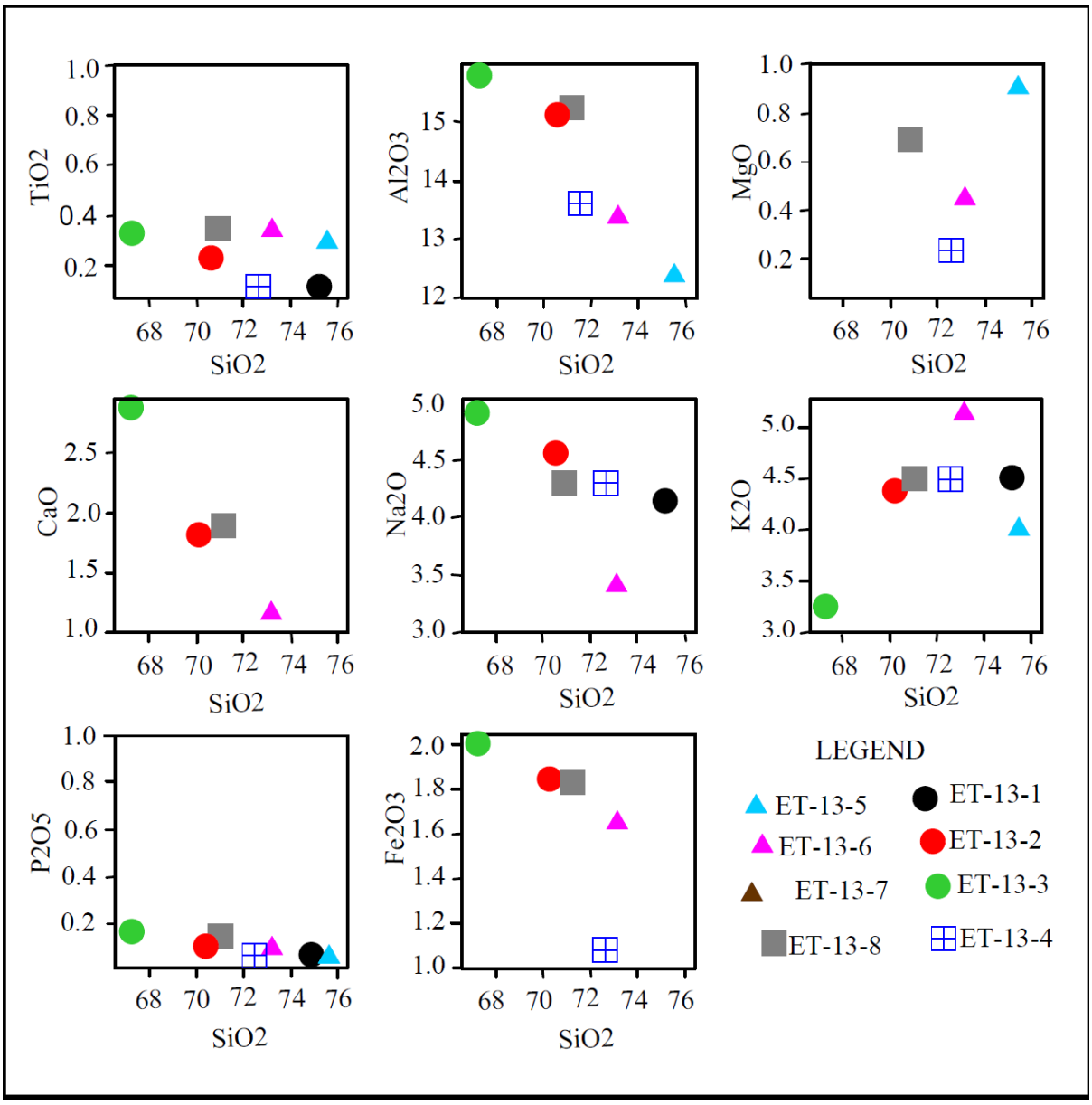

Fig. 19 Harker variation diagrams: Silica (SiO_2 wt. %) plotted against a range of major oxides (wt. %) showing the behavior of major elements against SiO_2 from the studied area

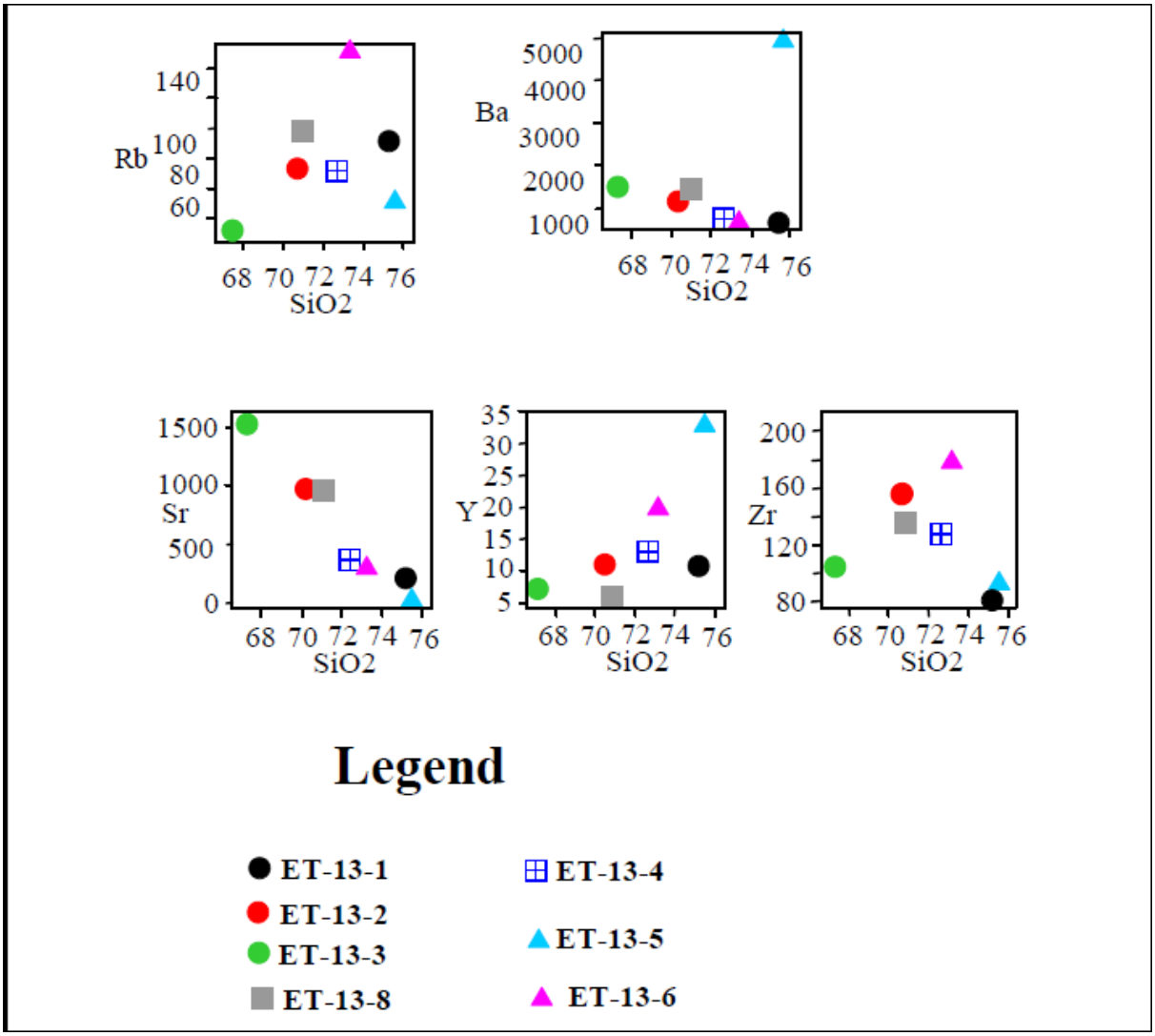

Fig. 20 Harker variation diagrams; Silica (SiO_2 in wt. %) plotted against selected trace elements (in ppm) for the granites and metavolcanic rocks from the studied area.

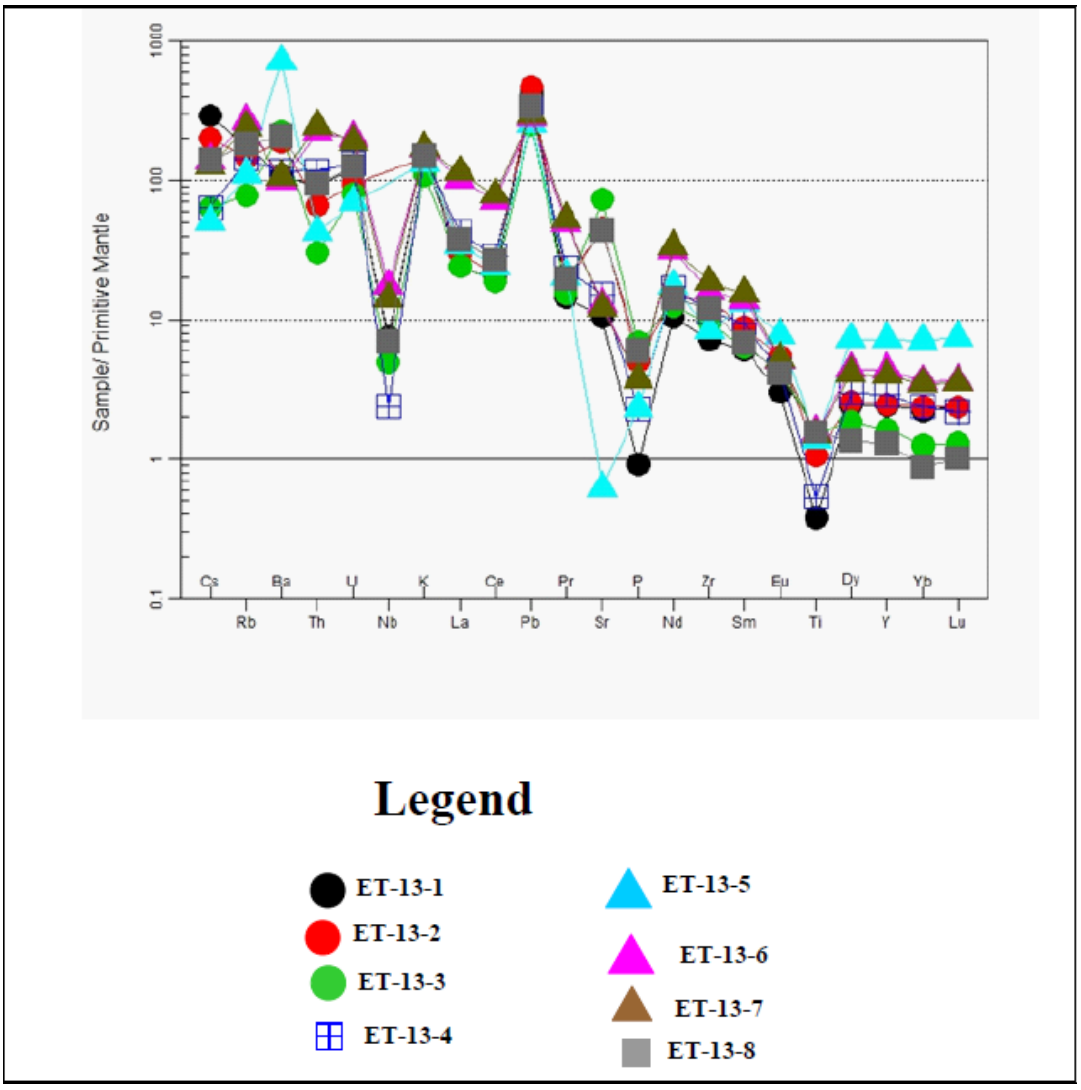

Fig. 21 Primitive Mantle –normalized multi-element diagram of granites and metavolcanics from the study area (Sun and McDonough, 1989)

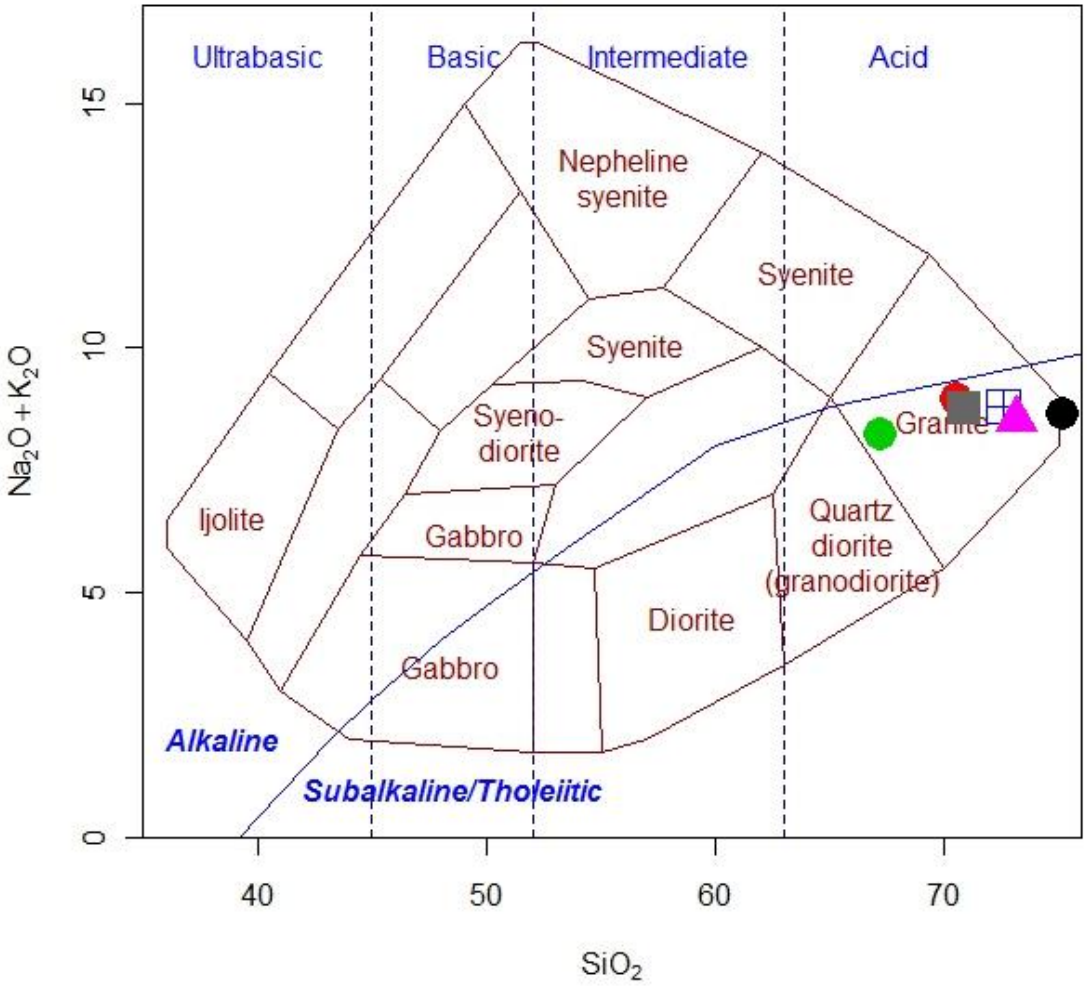

Fig. 22 chemical classification diagrams for the granitic rocks and metavolcanic rock based on TAS, wt. %, SiO_2 vs (Na_2O + K_2O) of (Cox et al., 1979), (Symbols same as Figure 21)

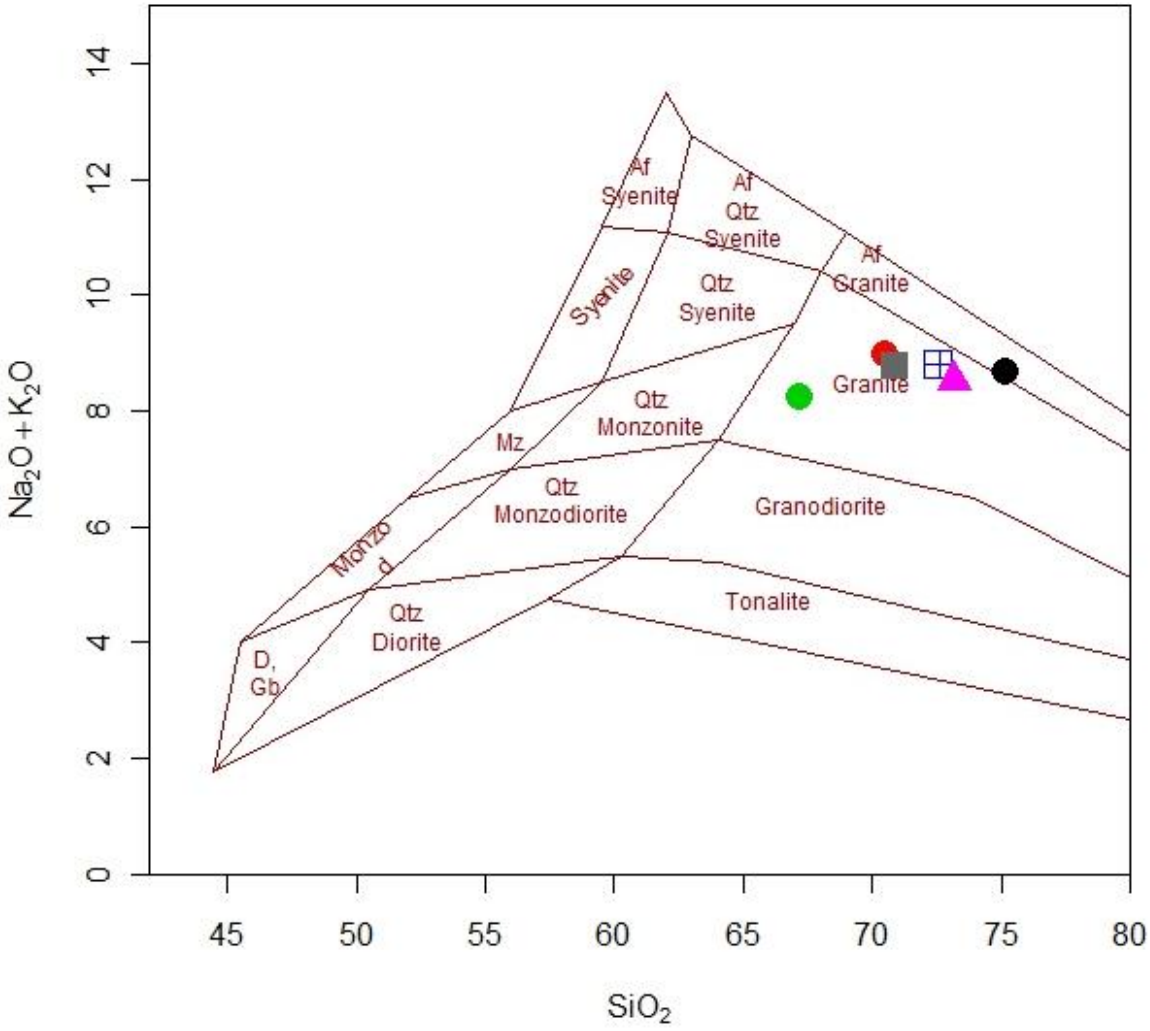

Fig. 23 chemical classification diagram for the granitic rocks and metavolcanic rock based on TAS (SiO_2 vs $Na_2O + K_2O$) of (Middlemost, 1994), (Symbols same as Figure 21)

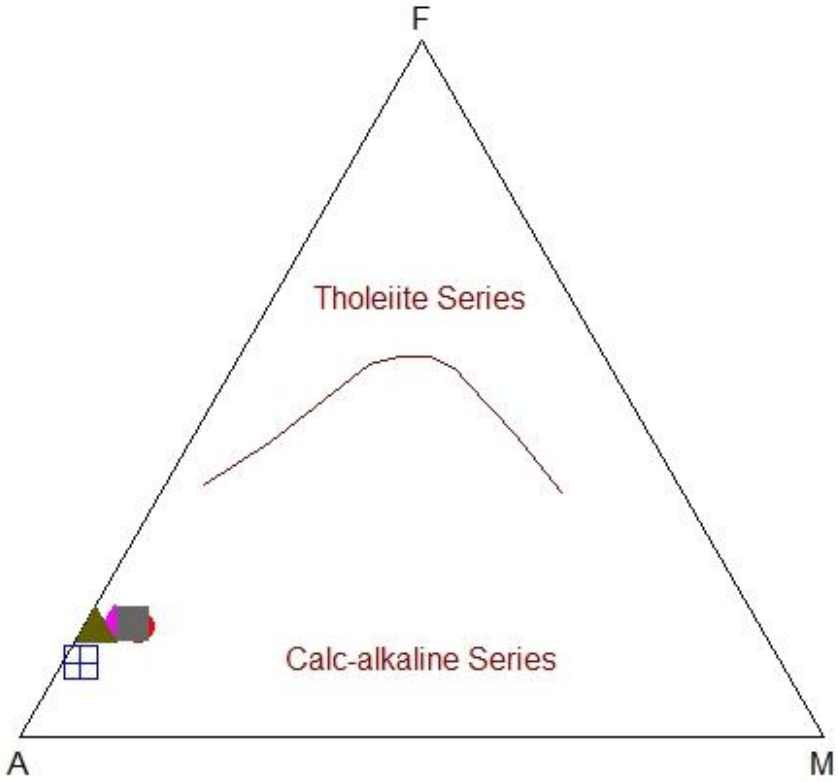

Fig. 24 AFM ternary diagram showing calcalkaline character of the granitoid and metavolcanic samples from the study area (Irvine & Baragar, 1971), (Symbols same as Figure 21)

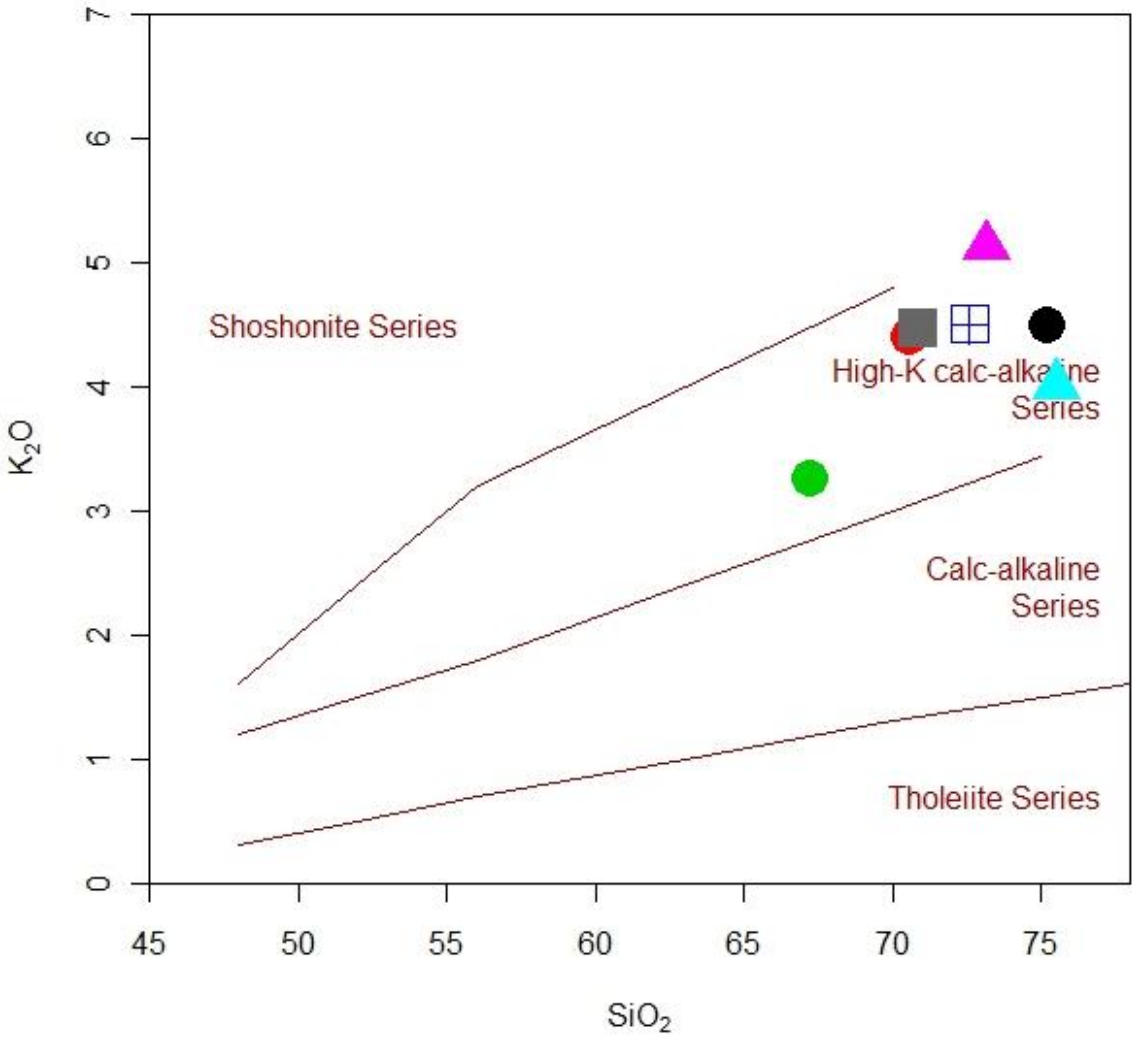

Fig. 25 the K_2O–SiO_2 plot showing High-K nature and slight shoshonitic series (Peccerillo and Taylor, 1976) of the granites and metavolcanic rock from the study area, (Symbols same as Fig. 21)

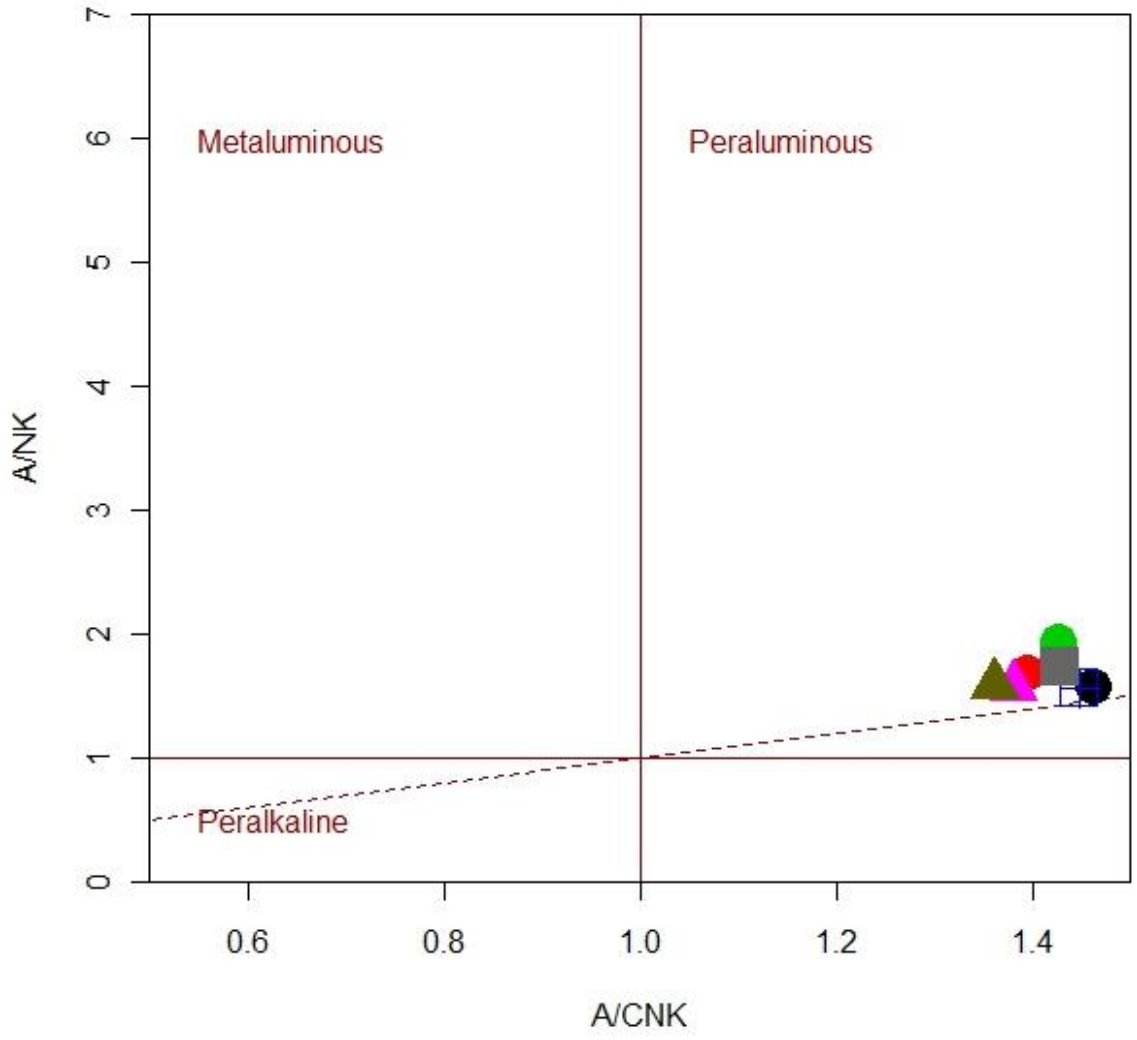

Fig. 26 A/CNK (Al_2O_3/ ($CaO+Na_2O+K_2O$) vs A/NK (Al_2O_3/ Na_2O+K_2O) plot (Shand, 1943) discriminating metaluminous, peraluminous and peralkaline compositions of the granites and metavolcanic rock samples from the study area, (Symbols same as Fig. 21)

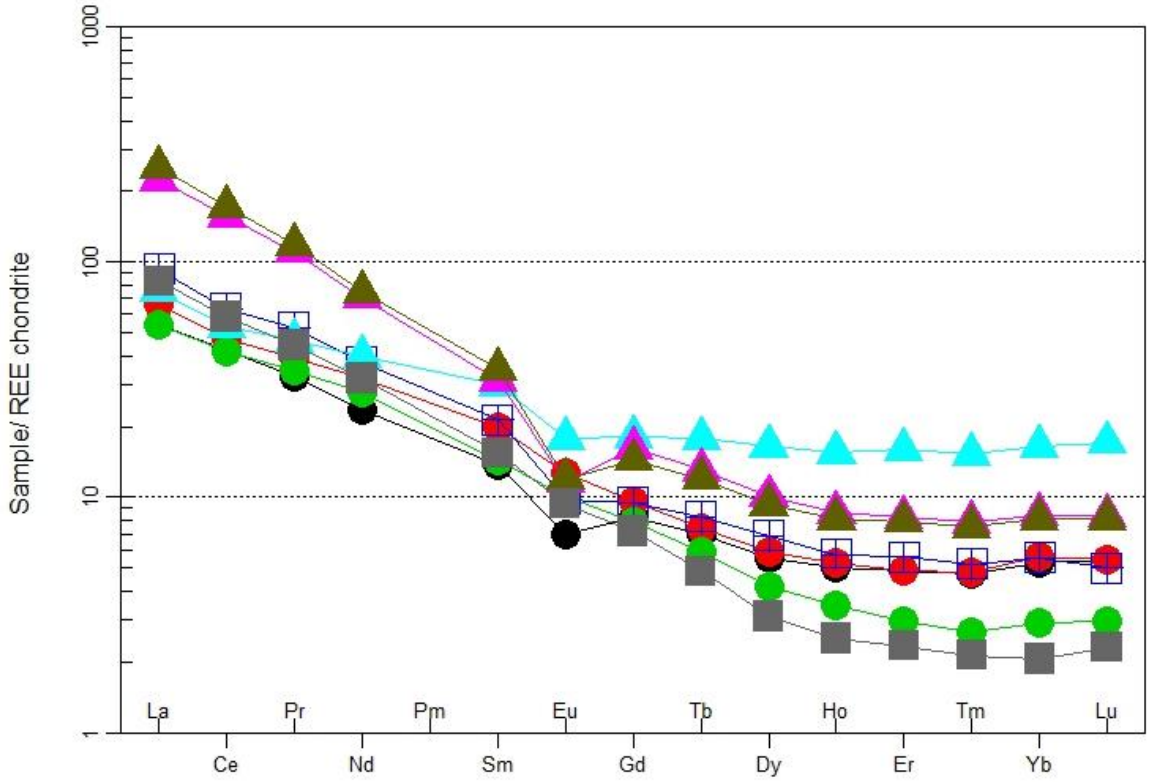

Fig. 27 Chonderite-normalized REE patterns from the studied area granites and metavolcanic (Boynton, 1984), (Symbols same as Fig. 21)

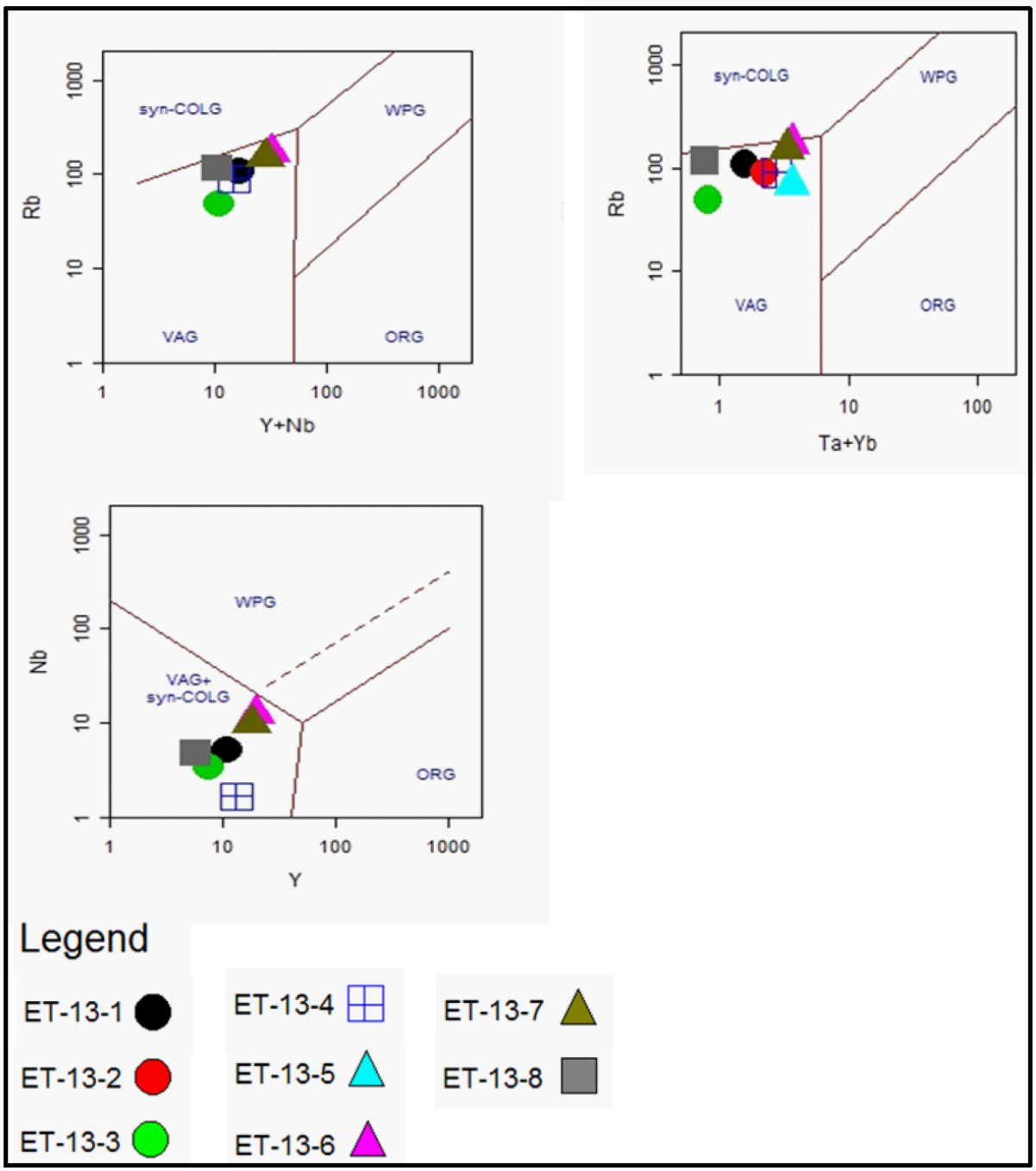

Fig. 28 Tectonic discriminant diagram of the samples from the studied area (after Pearce et al., 1984)

7. DISCUSSION

The results presented in the previous chapter will be discussed here. To illustrate the geochemistry (major elements, trace elements and rare earth elements) and U-Pb geochronology, several graphical plots have been generated and used. These various plots represent the results obtained from the different analytical methods.

The study area is situated within the north Ethiopian Precambrian shield terrain which represents the southernmost extension of the ANS. This region comprises largely of sutured low-grade assemblages of Neo-Proterozoic volcanic, volcano-sedimentary and sedimentary units, intrusives, and contains many remnants of oceanic crust (ophiolites) (Abdelsalam and Stern, 1996; Tadesse, 1996; and Tadesse-Alemu, 1998). The geology of the studied area mainly comprises metavolcanics, sericite quartz-feldspar schist, phyllitic and graphitic schist, mafic –ultramafic rocks, sedimentary rocks and granitic intrusives. The granitic intrusive suites intrude the arc assemblages in the area and are characterised by dark colored xenoliths. The granites were further traversed by younger aplitic dikes and basic dikes (dolerite) as observed in most I-type granitoids (John, 2000). Thrust and prominent lineaments were the major structural elements and have a resemblance to structures found in other parts of the ANS.

Single zircon evaporation Pb-Pb ages and conventional multi-grain U-Pb ages on zircon and titanite of the Nakfa intrusives yielded emplacement ages of (620- 640Ma) in Eritrea (Teklay et al., 2002) north of the studied area. The emplacement age of post tectonic Mai Kenetal granite was at 612.3±5.7 Ma (Avigad et al., 2007). The emplacement age of Mereb granite was at (606±0.9; 613.4±0.9; 608±7 Ma) (Miller et al., 2003; Asrat et al., 2004). (Asrat et al., 2004) proposed an emplacement age at 608 ± 7Ma (zircon U-Pb) for low-grade volcaniclastic sediments in the Negash pluton. (Finger et al., 2008) studied the post-tectonic granites at Aswan and found Ediacaran crystallization age which corresponds to 606±2 and 606–1 Ma. The Aswan granites contain no inherited zircon which is an important feature of S-type granites (Clemens, 2002).

As mentioned in the previous section, the U-Pb results for the studied area were based on multigrain zircon and titanite analyses. The U-Pb dating suggests that the mean emplacement age of the Hitsas granite is at about 627.5 ± 1.1 Ma (Fig.18a, b; Table 1) and that of the Gurungur granite is 624.24±0.60Ma (Fig. 18c; Table 1). The two granites vary only with 3 Ma suggesting similar emplacement time and are interpreted as older granites with no inherited zircon. The analysis of Kisad Gaba granite also yielded mean age of 606.1 ± 2.6 Ma

and 610.7 ± 1.1Ma (Fig. 18d, e; Table 1) and was interpreted as the youngest granitic intrusive with no inherited zircon which in turn confirms I-type character for these granites. The emplacement age of the Kisad Gaba granite was fairly close to that of Mai Kenetal, Mereb, Negash plutons in Tigray and Aswan granites. The Hitsas, Gurungur and Kisad Gaba granites are similar in age to that of Nakfa intrusives in Eritrea and Aswan granites in Egypt. These ages are also comparable to other granites in the juvenile Neoproterozoic crust of ANS or Pan-African orogen (900-500 Ma) (Asrat et al., 2004).

Based on the U-Pb data (Fig. 18; Table 1), the studied granites have no inherited zircon and the isotopic signatures indicate that these rocks are dominantly mantle-derived juvenile crust (Stern, 2002; Stoeser and Frost, 2006). This age reflects regional granitic melt generation in the lower crust of the thickened Ethiopian basement (Teklay et al., 2002). By this time, contractional deformation in Tigray had ceased, but the currently exposed metamorphic rocks lie at a depth of 6–8 km (e.g. Asrat et al., 2004). Therefore, the studied granites are consistent with previous findings (e.g., Asrat et al., 2004, Stern, 2002; Stoeser and Frost, 2006 and Teklay et al., 2002) with a substantial involvement of crustal materials.

In major element variation diagrams (Fig. 19), the studied samples form more or less well defined clusters and well defined trends, where Al_2O_3, Fe_2O_3, CaO, TiO_2, and P_2O_5 concentrations decrease with increasing SiO_2, suggesting commencement of plagioclase fractionation or magmatic differentiation trends (Clarke et al., 2005), whereas the concentration of Na_2O decreases with increasing SiO_2 and K_2O increases with increasing SiO_2 content. The total alkali concentrations are uniform within each sample (i.e., 8.22 – 8.97 wt. %). Decreasing Al_2O_3 with increasing silica indicates fractionation of aluminium-rich phases (plagioclase) (Clarke et al., 2005).The high SiO_2, (Na_2O + K_2O), and Al_2O_3, low MgO, Fe_2O_3, and CaO concentrations imply that the primary magma was derived from partial melting of the lower crust (Zhu et al., 2009). The concentration of P_2O_5 in I-type granites decreases with increasing SiO_2 (Fig. 19) showing that P_2O_5 in I-type granites is always low, which is consistent with decreasing solubility of Phosphorous in siliceous melts or removal of apatite(Chappell B.W., 1999; Sha and Chappell, 1999). The low P_2O_5 contents show similarity considering the individual samples (vary from 0.08-0.13%wt. %). These P_2O_5 concentrations are also similar geochemical character of low to intermediate P type that can be considered as fractionated I-type granitoids (Linnen and Cuney 2005). Therefore, the poor content of P_2O_5 (0.08-0.13%) in the studied samples suggests that the samples are I-type granites.

(Chappell and White, 1974 and 1992) distinguished S-type and I-type granites using different chemical parameters. I-types have relatively high sodium, Na_2O greater than 3.2%, in felsic

varieties, decreasing to more than 2.2% in mafic types. S-types have relatively low sodium, Na_2O normally less than 3.2% in rocks with approximately 5%K_2O, decreasing to less than 2.2% in rocks with approximately 2% K_2O. In addition, S-types have a Mol Al_2O_3/ (Na_2O+K_2O+CaO) ratio of greater than 1.1 and I-types less than 1.1. The authors recommended these criteria to be crucial in distinguishing I-type and S-type granites.

Accordingly, the data obtained in this study suggest that the samples are strongly peraluminous (A/CNK>1.36), high K_2O (3.27-5.19), low P_2O_5 (<0.13) that decreases with increasing SiO2 concentration (Fig.19) and high Na_2O (>3.2). These features are consistent with the S-type granites and differentiation trend of I-type granitic magmas respectively. S-type granites contain Al-rich minerals such as cordierite or muscovite; whereas I-type granites are metaluminous and always contain amphibole, (Chappell et al., 2012). The studied samples contain minor amount of hornblende and secondary muscovite, but no garnet or cordierite. Thus, the studied granites have S-type character and belong to I-type granites. The S-type characteristics are possibly due to the involvement of crustal materials (metasedimentary rocks) in the study area.

The high SiO_2 (67.21-75.51), total alkali concentrations ($8.22 \leq Na_2O + K_2O \leq 8.97$ %), and Fe_2O_3/MgO ratios (1.34-11.75) suggests that the studied granitic plutons and metavolcanic experienced significant magmatic differentiation. The low CaO/Na_2O ratios (0.16-0.57), higher Na_2O/K_2O ratios (0.08-1.51) and higher K_2O/ Na_2O ratios (0.97-1.55; Table 2) suggest that the samples are K_2O and Na_2O enriched, with the predominance of K_2O over Na_2O. Peraluminous I-type granites are probably resulted from fractional crystallization of hornblende (Cawthorn and Brown, 1976; Cawthorn et al., 1976) or from partial melting of mafic source rocks (Chappell et al., 2012). Therefore, the compositional variation of the granite samples and metavolcanic sample is possibly caused by varying degrees of partial melting and/or fractional crystallization/crustal contamination of magma in subduction related tectonics.

In the primitive mantle-normalised plot (Sun and McDonough, 1989), (Fig. 21) the studied samples are enriched in large ion lithophile elements (e.g., Pb, and K) and extremely depleted in high field strength elements (e.g., Nb, Ta and Ti). The drastic depletion in Nb, P and Ti is typical characteristics of subduction related granites (Pearce et al., 1984; Condie, 1998). The strong depletion in (P) may suggest a fractionation of apatite and the low Nb, Ta and Ti illustrates the separation of Ti-bearing phases such as Ilmenite or Rutile. The Ba, K and Pb are concentrated in felsic melts being derived from the partial melting of alkali feldspar

(Thompson et al., 1983). Thus, the high concentration of Ba in the samples from the studied area indicates a partial melting above subduction zones of volcanic arc tectonics.

The studied granites and metavolcanic are characterized by enrichment of large-ion lithophile elements (LILE) in contrast to more compatible, high field strength elements (HFSE), which in turn are indicative of arc-related magmatism/ subduction-related/and or calc-alkaline differentiation trend (Pearce et al., 1984). The significant enrichment in large ion lithophile elements (e.g., Ba, K, Pb) and light rare earth elements and depletion in high field strength elements (e.g., Nb, Ta) suggest an affinity with volcanic rocks from an island arc or active continental margin setting (Grove et al., 2003; Gill, 1981).

The ratio of K/Rb varies from (94.74 – 778) in the granites and is 738.57 in the metavolcanic:- The Ba/Sr ratio ranges between (0.99-3.50) in the granites and is 383.50 in the metavolcanic:- The ratio of Rb/Sr fall in the range of (0.03-0.62) in the granites and is 5.38 in the metavolcanic:- The Ba/Rb ratios range between (4.03-30.98) in the granites and is 71.21 in the metavolcanic (see Table 3). The variation in the incompatible element ratios of Ba/Sr, Ba/Rb, K/Rb, and Rb/Sr, for the granites and metavolcanic suggest partial melting, and are similar as observed in most continental crust high-K calc alkaline igneous suites (Bertrand et al., 1984; Ayuso et al., 1992). The studied samples are characterized by high K/Rb ratio (>100) except (sample ET-13-6) with K/Rb (94.74) from Kisad Gaba and low Rb/Sr ratio (<10) suggesting I-type characteristics. The Cr varies from150 -620ppm and Ni vary from 800-3430 ppm. Nickel has the highest concentrations of 3430, which is a very rare case to find in granites. Ni, Co, Cr Highly compatible elements and Ni, Co are concentrated in olivine, and Cr in spinel and clinopyroxene (From Winter, 2001). High concentrations indicate a mantle source or indicate a problem with analytical methods (i.e., during crushing).

The granite samples show high degree of fractionation with steep patterns in the Light Rare-Earth Elements (La to Sm) relative to Heavy Rare-Earth Elements (Gd to Lu) that displays varying degree of depletion in the study area. The studied samples are fractionated on the chonderite –normalized Rare Earth Elements with steep slopes (Fig. 27; Table 4). The samples are enriched in Light Rare-Earth Element relative to Heavy Rare-Earth Elements and have fractionated Rare Earth element patterns $(La/Yb)_N$ = 10.24–40.24).The similarities in the Light Rare-Earth Elements and Heavy Rare-Earth Elements patterns of the granites from the different areas indicate their similarity in origin (Odewumi et al., 2013).

The high (La_N/Yb_N (where N-denotes that the concentration is normalized to the chonderite abundance) values for the Hitsas granite (10.24 to 23.52,), Gurungur granite (16.86) and Kisad Gaba granite (26.67 to 40.24), suggest a significant LREE and HREE fractionation

(Taylor, 1965; Odewumi et al., 2013). The Rare earth element patterns (see Fig. 27; Table 4) show that the samples are fractionated and have LREE (Light Rare Earth Element) enrichment with (Ce_N/Sm_N = 2.36-4.99) compared to HREE (Gd_N/Yb_N= 1.56-3.48) with a significant positive Eu anomaly (Eu/Eu*= 6.98-13.06).

The high values of the Ce_N/Yb_N ratios (8.07 to 14.24) in Hitsas granite, (11.39) in Gurungur granite and (18.67 to 28.36) in Kisad Gaba granite, indicate that the Kisad Gaba granite had higher degree of fractionation than the Hitsas and Gurungur granite:- The La_N/Sm_N ratio (3.32 to 3.90) in Hitsas granite, (4.39) in Gurungur granite and (7.14 to 7.23) in Kisad Gaba granite suggest that the Kisad Gaba samples are highly fractionated than the other samples. Thus, the enrichment in the Light Rare-Earth Elements (LREE) relative to Heavy Rare-Earth Elements (HREE) in all the samples suggests a higher degree of fractionation (Odewumi et al., 2013).

The chemical affinity of the studied granites and one metavolcanic is illustrated by plotting the SiO_2-Feot/MgO (after Miyashiro, 1974), (Fig. not shown), and SiO_2-K_2O plot (Peccerillo and Taylor, 1976), (see Fig. 25). In fig.25 it is shown that all samples are clustered in the high-k calcalkaline field suggesting their calc-alkaline affinity. On the AFM plot (Irvine and Baragar, 1971), (see Fig. 24) all data are clustered in the calc-alkaline field showing their enrichment in alkali (Na_2O+K_2O) oxides. Alumina saturation index diagram (Shand, 1943; see Fig. 26) shows that the granites and metavolcanic samples from the study area are exclusively peraluminous as indicated by the values of A/CNK = in the granitic rocks (1.36-1.46) and in the metavolcanic rock (2.77) and values of A/NK= in the granitic rocks (1.56-1.92), and in the metavolcanic rock (2.85); where A: Al_2O_3, CNK: CaO+ Na_2O+K_2O respectively. It is worth noting that these values are greater than 1.1 (see discussion in page 62).

The constructed tectonic-setting discrimination diagram (Pearce et al., 1984) shows that the studied samples are associated with subduction zones (volcanic arc) and syn and post-collisional granites (Fig. 28). In the study area, the characteristic features of the granitic and metavolcanic rocks from the different areas are their depletion in Nb, P, Ta and Ti, and enrichment in most incompatible elements (K, Rb, Sr, Ba, U, Pb and Th) compared to highly charged elements that resulted in magmatic fractionation trends. The trace and Rare Earth Elements display characteristics features usually attributed to magmatic arc calc-alkaline granitoids; the enrichment in large ion lithophile elements and depletion in high field strength elements (e.g., Nb, Ta, and Ti) that imply a significant amount of crust material was involved in their genesis most probably as a result of magma mixing (Pearce et al., 1984).

The result from this study which integrates isotopic data, geological data, and geochemical data reveal that the studied samples are I-type and have S-type characteristics showing the involvement of significant crustal material in their genesis, most probably from partial melting of crustal materials or magma mixing (juvenile crust) evidenced by the wide spread occurrence of mafic enclaves in the granitic plutons.

8. CONCLUSIONS

Based on the integration of U-Pb isotopic data, geochemical data, petrographic data and geological data of the Neoproterozoic granitic and metavolcanic rocks of southernmost ANS, Northern Ethiopia, western shire district, the following conclusions can be drawn:

(1) The study area consists of low-grade metavolcano-sedimentary rock assemblages that belong to the Tsaliet and Tambien Groups of the Arabian-Nubian Shield. Six major lithological units have been identified in the area and include mainly metavolcanics, sericite quartz-feldspar schist, phyllitic and graphitic schist, mafic -ultramafic rocks, sedimentary rocks, and granitic intrusives. The main mineralizations are placer gold and volcanogenic massive sulfides. The granite suites are dominantly represented by grey and pink granites, which are traversed by younger aplitic dikes, basic dikes (dolerite dike) which are common character of I-type granites. The wide spread occurrence of mafic enclaves in the granitic plutons (presence of dark colored xenoliths) suggest their derivation from mantle.

(2) Petrographically, the groundmass of the rock samples is mainly composed of plagioclase, quartz, and K-feldspars (Microcline, perthitic), biotite and secondary muscovite, hornblende. Accessory minerals include; zircon, allanite, apatite, rutile, titanite, pyrite and common Fe-Ti oxides (Ilmenite and magnetite).

(3) Zircon and titanite U-Pb age dates indicate that the Hitsas pluton is emplaced at about 627.5 ± 1.1 Ma, that of the Gurungur granite is at about 624.24±0.60Ma, and that of the Kisad Gaba granite is at about 606.1 ± 2.6 Ma and 610.7 ± 1.1Ma coeval with the juvenile Neoproterozoic rocks in the ANS. All the zircon grains were free of inheritance/inherited zircon cores/, which is an important feature of S-type granites (Clemens, 2002). This lack of inheritance confirms that the studied granites are clearly I-type.

(4) The geochemical data indicates that the higher Na_2O/K_2O ratios (0.08-1.51) and higher K_2O/ Na_2O ratios (0.97-1.55; Table 2) suggest that the samples are K_2O and Na_2O dominated, with the predominance of K_2O over Na_2O. The P-poor (P_2O_5<0.13wt %), high SiO_2 (67.21-75.51), high total alkali concentration (8.22-8.97wt %) and show high-K calc-alkaline affinity formed during volcanic arc magmatism/subduction related / environments. The high SiO_2, (Na_2O + K_2O), and Al_2O_3, low MgO, Fe_2O_3, and CaO concentrations imply that the primary magma was

derived from partial melting that involves lower crust. The compositional trends of the granites and metavolcanic rocks indicate a decrease in Al_2O_3, Fe_2O_3, MgO, CaO, TiO_2, P_2O_5, with increasing SiO_2, which might be due to the fractionation of plagioclase or biotite or crustal contamination of magmas during magmatic emplacement.

(5) The constructed discrimination diagrams and spider diagrams together with the geochemical characteristics of high-K calcalkaline affinity, their I-type and S-type character with strongly peraluminous (A/CNK= 1.36-1.46 in the granites and 2.77 in the metavolcanic), the enrichment of large ion lithophile elements, depletion in high field strength elements (Nb, Ta and Ti) and P signifying a magmatic tectonics above subduction zones of volcanic arc and syn to post-collisional granitoids.

(6) Thus based on the integration of the geological data, geochemical data and geochronological (U-Pb zircon and titanite) data the studied granites and metavolcanic rocks are typically Neoproterozoic I-type and have S-type characteristics with strongly peraluminous nature at western Shire (Hitsas, Gurungur and Kisad Gaba areas). They are generated from a mixed mantle-crust source. The negative Nb, Ti, and P anomalies most probably formed by partial melting of crustal materials or magma mixing (juvenile crust) or indicate a subduction zone related origin. The I-type granitoids are also enriched in Ba, K, Th, and U and depleted in Nb indicating they had interaction with the crust. I-type granitoids might result from contamination of mantle derived magmas by continental crust materials above subduction zones or volcanic arc, evidenced by the wide spread occurrence of mafic enclaves in the granitic plutons.

9. REFERENCES

Abdelsalam, M.G., and Stern, R.J., 1996. Sutures and shear zones in the Arabian–Nubian Shield. Journal of African Earth Science. 23, 289–310.

Alemu, T., 1998. Geochemistry of Neoproterozoic granitoids from Axum Area, northern Ethiopia. Journal of African Earth Sciences 27, 437-460.

Alene, M., 1998. Tectonomagmatic evolution of the Neoproterozoic rocks of the Mai-Kenetal-Negash area, Tigrai, northern Ethiopia. Unpublished Ph.D. Thesis, University of Turin, Italy.

Alene, M., Jeniken, G.R.T., Leng, M. J., and Darby shire, F.D.P., 2006. The Tambien Group, Ethiopia: An early Cryogenian (ca. 800 - 735 Ma) Neoproterozoic sequence in the Arabian-Nubian Shield. Precambrian Research 147, 79-99.

Alene, M., Ruffini, R., and Sacchi, R., 2000. Geochemistry and geotectonic setting of Neoproterozoic rocks from northern Ethiopia (Arabian-Nubian Shield). Gondwana Research 3, 333-347.

Andersson, U.B., Ghebreab, W., and Teklay, M., 2006. Crustal evolution and metamorphism in east-central Eritrea, south-east Arabian-Nubian Shield. Journal of African Earth Sciences 44, 45-65.

Asrat, A., and Barbey, P., 2003. Petrology, geochronology and Sr–Nd isotopic geochemistry of the Konso pluton, south-western Ethiopia: implications for transition from convergence to extension in the Mozambique Belt. International journal of Earth science, 92:873–890.

Asrat, A., Barbery, P., and Gleizes, G., 2001. The Precambrian geology of Ethiopia: a review. Africa Geoscience review, 8: 271-288.

Asrat, A., Barbery, P., and Gleizes, G., 2001. The Precambrian geology of Ethiopia: a review. Africa Geoscience review, 8: 271-288.

Asrat, A., and Barbey, P., 2003. Petrology, geochronology and Sr–Nd isotopic geochemistry of the Konso pluton, south-western Ethiopia: implications for transition from convergence to extension in the Mozambique Belt. International journal of Earth science, 92:873–890.

Asrat, A., P. Barbey, J. N. Ludden, L. Reisberg, G. Gleizes and D. Ayalew, 2004. Petrology and Isotope Geochemistry of the Pan-African Negash Pluton, Northern Ethiopia: Mafic---Felsic Magma Interactions During the Construction of Shallow-level Calc-alkaline Plutons. Journal of Petrology., v. 45, 1147–1179.

Ayalew, T., Bell, K., Moore, J.M., and Parrish, R.R., 1990. U-Pb and Rb-Sr geochronology of the Western Ethiopian Shield. Geological Society America Bulletin 102, 1309-1316.

Avigad, D., Stern, R.J., Beyth, M., Miller, N., and McWilliams, M.O., 2007. Detrital zircon U-Pb geochronology of Cryogenian diamictites and Lower Paleozoic sandstone in Ethiopia (Tigray): Age constraints on Neoproterozoic glaciation and crustal evolution of the southern Arabian-Nubian Shield. Precambrian Research 154, 88-106.

Ayuso, R., and Arth, J.G., 1992. The Northeast Kingdom batholith, Vermon: magmatic evolution and geochemical constraints on the origin of Acadian granitic rocks. Contribution to Mineralogy and Petrology, vol. 111, pp. 1-23.

Azevedo, M.R., and Nolan, J., 1998. Hercynian late-post-tectonic granitic rocks from the Fornos de Algodres area (Northern Central Portugal): Lithos, v. 44, 1-20.

Barrie, C.Tucker, William Nielson, F and Claude Aussant, H 2007. The Bisha Volcanic Associated Massive Sulfide Deposit, Western Nakfa Terrane, Eritrea. Economic Geology, 102: 717–738.

Bell, A. M., 1981. Vergence: an evaluation J structural. Geol., **3**, 197-202.

Berhe, S.M., 1990. Ophiolites in Northeast and East Africa: implications for Proterozoic crustal growth. Journal of Geological Society of London 147, 647-657.

Berth, D., Choukroune, P. and Jegouzo, P., 1979. Orthogenesis mylonite and non-coaxial deformation of granites: the example from south Armorican shear zone. J. Structural geol. **1**, 31-42.

Bertrand, J.M., Dupuy, C., Dostal, J., and Davidson, I., 1984. Geochemistry and geotectonic interpretation of granitoids from Central Iforas (Mali, West Africa). Precambrian Research, vol. 26, pp. 265-283.

Beyth, M., 1972a. The geology of central – western Tigray, PhD. Thesis, Rheinche Friedrich–Wilhems Universitate, Bonn, Germany, 159 pages.

Beyth M., 1972b. Palaeozoic-Mesozoic sedimentary basin of Mekele Outlier, Northern Ethiopia. AAPG Bull. 56, 2426-2439.

Beyth, M., Avigad, D., Wetzel, H.U., Mattews, A., and Berhe, S.M., 2003. Crustal exhumation and indications for Snowball Earth in the East African Orogen: north Ethiopia and east Eritrea. Precambrian Research 123, 187-201.

Boynton, W.V., 1984. Geochemistry of Rare Earth Elements: Meteoritic Studies. Elsevier, Amsterdam, pp: 63-114.

Cawthorn, R.G., Strong, D.F., Brown, P.A., 1976. Origin of corundum-normative intrusive and extrusive magmas. Nature 259, 102–104.

Cawthorn, R.G., Brown, P.A., 1976. A model for the formation and crystallization of corundum-normative calc-alkaline magmas through amphibole fractionation. Journal of Geology 84, 467–476.

Chappell, B.W., White, A.J.R., 1974. Two contrasting granite types. Pac. Geol. 8, 173– 174.

Chappell, B.W., Bryant, C.J., Wyborn, D., White, A.J.R., and Williams., I.S., 1998. High and low Temperature I-type granites. Resource Geology, 48: 225-236.

Chappell, B.W., White, A.J.R., 1992. I- and S-type granites in the Lachlan Fold Belt. Transactions of the Royal Society of Edinburgh: Earth and Environmental Science 83, 1–26.

Chappell, B.W., Bryant, C.J., Wyborn, D., 2012. Peraluminous I-type granites. Lithos 153, 142–153.

Clarke, D.B., Henry, A.S., and Hamilton, M.A., 2005. Composition, age, and origin of granitoid rocks in the Davin Lake area, Rottenstone Domain, Trans-Hudson Orogen, northern Saskatchewan: Canadian Journal of Earth Sciences, v. 42, p. 599-633.

Clemens J.D., 2002. S-type granitic magmas—petrogenetic issues, models and evidence. Earth-Science Reviews 61, 1 –18.

Condie, K.C., 1998. Plate Tectonics and Crustal Evolution. Butterworth-Heinmann, London, pp: 69.

Corfu, F., 2004. U-Pb age, setting, and Tectonic significance of the anorthosite –mangerite-charnockite-granite suite, Lofoten-Vesterålen, Norway: journal of Petrology, v.45, p. 1799-1819.

Cox, K.G., Bell, J.D. and Pankhurst, R.J., 1979. The interpretation of igneous rocks. Allen and Unwin, London, pp. 450.

Debon, F. and Lefort, P., 1983. A chemical mineralogical classification of common-plutonic rocks and associations. Trans. Roy. Soc. Edinburgh, Earth Sci., V. 73, pp. 135–149.

De Wit, M.J., 1981. Precambrian base metals. In: Chewaka, S., and de Wit, M.J. (eds.), Plate tectonics and metallogenesis: some guidelines to Ethiopian Mineral Deposits, Ethiopian Institute of Geological Surveys Bulletin 2, 65-82.

Ethiopian Metrological Service Agency, 2012.

Finger F, Dörr W, Gerdes A, et al., 2008. U-Pb zircon ages and geochemical data for the Monumental Granite and other granitoid rocks from Aswan, Egypt: implications for the geological evolution of the western margin of the Arabian-Nubian Shield. Miner Petrol; 93: 153-83.

Gass, I.G., 1981. Pan African (Upper Proterozoic) plate tectonics of Arabian-Nubian Shield. In: Precambrian plate tectonics. Elsevier, Amsterdam, 387-405.

Gebresillassie, S., 2009. Nature and characteristics of metasedimentary rock hosted gold and base metal mineralization in the Workamba area, central Tigray, northern Ethiopia. PhD thesis, Ludwig Maximilians, Munich University, Germany, 148 pages.

Harker, A., 1909. The Natural History of Igneous rocks. Macmillan, New York.

Harvest, 2010. Regional geology of Asgede concession, Northern Ethiopia (Unpublished report)

Irvine, T .N., and Baragar, W.R.A., 1971. A guide to the chemical classification of the common volcanic rocks. Can. Jour. Earth Sci., v.8, 523-548.

John, C., 2000. The Geology and mapping of granite batholiths. Springer-Verlag, Berlin, Heidelberg, 96, 147 pages.

John, D. Winter., 2001. An Introduction to Igneous and Metamorphic Petrology. Prentice Hall.

Johnson, P.R., Andresen, A., Collins, A.S., Fowler, A.R., Fritz, H., Ghebreab, W., Kusky, T., and Stern, R.J., 2011. Late Cryogenian–Ediacaran history of the Arabian–Nubian Shield: A review of depositional, plutonic, structural, and tectonic events in the closing stages of the northern East African Orogen. Journal of African Earth Sciences, Volume 61, Issue 3,167-232.

Johnson, P.R, 2014. An Expanding Arabian-Nubian Shield Geochronologic and Isotopic Data set: Defining Limits and Confirming the Tectonic Setting of a Neoproterozoic Accretionary Orogen. The Open Geology Journal, 2014, 8, (Suppl 1: M2) 3-33.

Kazmin, V., 1971. Precambrian of Ethiopia. Nature, 230, 176-177.

Kazmin, V., 1975. The Precambrian of Ethiopia and some aspects of the Geology of the Mozambique Belt. Bulletin Geophysics. Obs., Addis Ababa University 15, 27-43.

Kazmin, V., Shiferaw, A., and Balcha, T., 1978. The Ethiopian basement and possible manner of evolution, Geologische Rundschau 67, 531-546.

Krogh, T. E., 1973. A low contamination method for hydrothermal decomposition of zircon- and extraction of U and Pb for isotopic age determinations. Geochim Cosmochim

Acta 37: 485–494

Krogh, T. E., 1982. Improved accuracy of U-Pb ages by the creation of more concordant-systems using an air abrasion technique. Geochim Cosmochim Acta 46: 637–649

Kröner, A., 2001. The Mozambique belt of East Africa and Madagascar: significance of zircon and Nd model ages for Rodinia and Gondwana supercontinent formation and dispersal. South African Journal of Geology 105, 151–167.

Kröner, A., Linnebacher, P., Stern, R.J., Reischmann, T., Manton, W., and Hussein, I.M., 1991. Evolution of Pan-African island arc assemblages in the southern Red Sea Hills, Sudan, and in south-western Arabia as exemplified by geochemistry and geochronology. Precambrian Research 53, 99-118.

Küster, D., 2008. Granitoid-hosted Ta mineralization in the Arabian–Nubian Shield: Ore deposit types, tectono-metallogenetic setting and petrogenetic framework. Ore Geology Reviews 35, 68–86.

Küster, D., and Harms, U., 1998. Post-collisional potassic granitoids from the southern and north-western parts of the Late Proterozoic east African Orogeny: a review. Lithos 45, 177–195.

Küster, D., Romer, R.L., Tolessa, D., Zerihun, D., Bheemalingeswara, K., Melcher, F., and Oberthür, T., 2009. The Kenticha rare-element pegmatite, Ethiopia: internal differentiation, U–Pb age and Ta mineralization. Miner Deposita, 44:723–750.

Ludwig, K. R., 2003, Isoplot 3.0. A geochronological tool kit for Microsoft Excel: Berkeley Geochronology Center Special Publication No. 4, 70 p.

Middlemost, E. A. K., 1994. Naming materials in the magma/igneous rock system. Earth Sci Rev 37:215-224.

Miller, N.R., Alene, M., Sacchi, R., Stern, R.J., Conti, A., Kröner, A., and Zuppi, G., 2003. Significance of the Tambien Group (Tigray, N. Ethiopia) for Snowball Earth events in the Arabian–Nubian Shield. Precambrian Research 121 263–283.

Miller, N.R., Stern, R.J., Avigad, D., Beyth, M., and Schilman, B., 2008. Cryogenian slate-carbonate sequences of the Tambien Group, Northern Ethiopia. Precambrian Research.1-8.

Miyashiro, A., 1974. Volcanic rock series in island arcs and active continental margins. American Journal of Sciences., 274: 321-355.

Odewumi SC, Olarewaju VO (2013) Petrogenesis and Geotectonic Settings of the Granitic Rocks of Idofin-osi-eruku Area, Southwestern Nigeria using Trace Element and Rare Earth Element Geochemistry. J Geol Geosci 2: 109.

Pearce, J.A., Harris, N.B.W. and Tindle, A.G., 1984. Trace element Discrimination Diagrams for the Tectonic Interpretation of Granitic Rocks. Journal of petrology, v .25, pp.956-983.

Peccerillo, A., and Taylor S .R., 1976. Geochemistry of Eocene calc-alkaline volcanic rocks from the Kastamonu area, Northern Turkey. Contrib Mineral Petrol 58: 63-81.

Roobol, M. J., Ramsay, C. R., Jackson, N. J and Darbyshire, P. F. 1983. Late Proterozoic lavas of the Central Arabian Shield-evolution of an ancient arc system. Journal of the Geological Society, London 140: 185-202.

Sajona, F.G., Maury, R.C., Bellon, H., Cotton, J., and Defant, M., 1996. High field strength elements of Pliocene Pleistocene island-arc basalts Zamboanga Peninsula, Western Mindanao (Philippines). Petrology, 37: 693-726.

Shackleton R.M., 1986. Precambrian collision tectonics in Africa. In: collision tectonics-Geological Society London, Special publication 19, 329-341.

Shand, S.J., 1943. Eruptive Rocks. Their Genesis, Composition, Classification, and Their Relation to Ore-Deposits with a chapter on Meteorite. John Wiley and Sons., New York, pp. 444.

Simpson,C. and Schmid, S. M., 1983. An evaluation of criteria to deduce the sense of movement in sheared rocks. Bulletin, Geol. Soc. America 94, 128-588.

Stacey, J.S., Kramers, J.D., 1975. Approximation of terrestrial lead isotope evolution by a two-stage model. Earth Planet. Sci. Lett. 26, 207–221.

Stern, R.J., 1994. Arc assembly and continental collision in the Neoproterozoic east African orogen: implication for the consolidation of Gondwanaland. Annual review Earth planetary science 22,319-351.

Stern, R.J., and Abdelsalam, M.G., 1998. Formation of juvenile continental crust in the Arabian-Nubian Shield: Evidence from granitic rocks of the Nakasib suture, NE Sudan. Geologische Rundschau 87, 150-160.

Stern, R.J., 2002. Crustal evolution in the East African Orogen: a neodymium isotope Perspective. Journal of African Earth Sciences 34, 109-117.

Stoeser DB, Frost CD. Nd, Pb, Sr, and O isotopic charcterization of Saudi Arabian Shield terranes. Chem Geol 2006; 226: 163-88.

Sun, S., and McDonough, W.F., 1989. Chemical and isotopic systematics of oceanic basalts: implications for mantle composition and processes: In Sunders, A.D., and Norry, M.J. (eds), Magmatism in ocean basins, Geological Society Special Publication No. 42, 313-345.

Tadesse, A., 1998. Geochemistry of Neoproterozoic granitoids from Axum Area, northern Ethiopia. Journal of African Earth Sciences 27, 437-460.

Tadesse, T., 1996. Structure across a possible intra-oceanic suture zone in low-grade Pan African rocks of northern Ethiopia. Journal of African Earth Sciences 23, 575-381.

Tadesse, T., 1997. Geology of the Axum area. Ethiopian institute of geological survey, memoir no 9, 147 pages.

Tadesse, T., Hoshino, M., and Sawada, Y., 1999. Geochemistry of low-grade metavolcanic rocks from the Pan-African of the Axum area, northern Ethiopia. Precambrian Research 99,101-124.

Tadesse, T., Hoshino, M., Suzuki, K., and Iisumi, S., 2000. Sm-Nd, Rb-Sr, and Th-U-Pb zircon ages of syn-and post-tectonic granitoids from the Axum area of northern Ethiopia. Journal of African Earth Sciences 30, 313-327.

Taylor S., 1965. The application of trace element data to problems in petrology. Physics and Chemistry of the Earth 6: 133-213.

Teklay, M., Kröner, A., and Mezger, K., 2002. Enrichment from plume interaction in the generation of Neoproterozoic arc rocks in northern Eritrea: implications for crustal accretion in the southern Arabian-Nubian Shield. Chem Geology 184, 167-184.

Teklay, M., Kröner, A., Mezger, K., and Oberhansli, R., 1998. Geochemistry, Pb-Pb single Zircon ages and Nd-Sr isotope composition of Precambrian rocks from southern and Eastern Ethiopia: implications for crustal evolution in East Africa. Journal of African Earth Sciences, 26, 207-227.

Tesfaye, K., Christian, K., and Friedrich, K., 1999. Geology, geochemistry and petrogenessis of intrusive rocks of the Wollega area, western Ethiopia. Journal of African earth science, volume 29, 715-734.

Thompson RN, Morrison MA, Dickin AP, Hendry GL (1983) Continental flood basalts - Arachnids rule OK? In: Hawkes- worth C J, Norry MJ (eds) Continental basalts and mantle xenoliths, Shiva Publishing Ltd. Cheshire, UK, pp 158-185.

Vail, J.R., 1985. Pan-African (late Precambrian) tectonic terranes and the reconstruction of the Arabian-Nubian Shield. Geology 13, 839-842.

Zhu, DiCheng., MO XuanXue, WANG LiQuan, ZHAO ZhiDan, NIU Yaoling, ZHOU ChangYong & YANG YueHeng, 2009. Petrogenesis of highly fractionated I-type granites in the Zayu area of eastern Gangdese, Tibet: Constraints from zircon U-Pb geochronology, geochemistry and Sr-Nd-Hf isotopes. Science in China press, Springer.